CLOUD TOP PROPERTIES AND CLOUD PHASE ALGORITHM THEORETICAL BASIS DOCUMENT

Paul Menzel
NOAA/NESDIS
Cooperative Institute for Meteorological Satellite Studies
University of Wisconsin - Madison

Kathleen Strabala
Cooperative Institute for Meteorological Satellite Studies
University of Wisconsin - Madison

(August 1996, version 4)

Table of Contents

1.0	Introduction	2
2.0	Overview	4
3.0	Algorithm Description	5
3.1	Theoretical Description	5
3.1.1.a	Physics of Cloud Top Properties Algorithm	5
3.1.1.b	Physics of Cloud Phase Algorithm	8
3.1.2.a	Mathematical Application of Cloud Top Properties Algorithm	11
3.1.2.b	Mathematical Application of Cloud Phase Algorithm	13
3.1.3.a	Estimate of Errors of Cloud Top Properties Algorithm	16
3.1.3.b	Estimate of Errors of Cloud Phase Algorithm	27
3.2	Practical Considerations	29
3.2.1	Numerical Considerations	29
3.2.2	Programming Considerations	30
3.2.3	Validation	32
3.2.4	Quality Control	40
3.2.5	Exception Handling	41
3.2.6	Data Dependencies	41
3.2.7	Output Product	44
3.3	References	45
4.0	Assumptions	48

1.0 Introduction

Cloud top properties (height, temperature, and effective emissivity) will be generated using the CO_2 slicing algorithm that corrects for possible cloud semi-transparency. The MODIS infrared CO_2 channels will be used to investigate clouds at 5 x 5 pixel resolution (Level 2) and to generate a global cloud climatology at .5 degree resolution (Level 3). At nadir one pixel has one km resolution. Additionally, cloud phase will be obtained by MODIS 8, 11 and 12 micron brightness temperature differencing at 5 x 5 pixel resolution (Level 2), and temporally averaged at .5 degree resolution (Level 3). This infrared technique will eventually be supplemented during daytime by the visible reflection function technique (King et al., ATBD-MOD-05) to result in a single MODIS cloud phase product. This document describes both algorithms, details the MODIS applications, and sizes the possible errors. Several references are available for further reading; for cloud top properties they are

Chahine, M. T., 1974: Remote sounding of cloudy atmospheres. I. The single cloud layer. J. Atmos. Sci., 31, 233-243.

Eyre, J. R., and W. P. Menzel, 1989: Retrieval of cloud parameters from satellite sounder data: A simulation study. J. Appl. Meteor., 28, 267-275.

Menzel, W. P., W. L. Smith, and T. R. Stewart, 1983: Improved cloud motion wind vector and altitude assignment using VAS. J. Clim. Appl. Meteor., 22, 377-384.

Menzel, W. P. and K. I. Strabala, 1989: Preliminary report on the demonstration of the VAS CO_2 cloud parameters (cover, height, and amount) in support of the Automated Surface Observing System (ASOS). NOAA Tech Memo NESDIS 29.

Menzel, W. P., D. P. Wylie, and K. I. Strabala, 1992: Seasonal and Diurnal Changes in Cirrus Clouds as seen in Four Years of Observations with the VAS. J. Appl. Meteor., 31, 370-385.

Menzel, W. P., D. P. Wylie, and K. I. Strabala, 1993: Trends in Global Cirrus Inferred from Four Years of HIRS Data. Technical Proceedings of the Seventh International TOVS Study Conference held 10-16 February in Igls, Austria.

Smith, W. L., and C. M. R. Platt, 1978: Intercomparison of radiosonde, ground based laser, and satellite deduced cloud heights. J. Appl. Meteor., 17, 1796-1802.

Wielicki, B. A., and J. A. Coakley, 1981: Cloud retrieval using infrared sounder data: Error analysis. J. Appl. Meteor., 20, 157-169.

Wylie, D. P., and W. P. Menzel, 1989: Two years of cloud cover statistics using VAS. J. Clim., 2, 380-392.

Wylie, D. P., W. P. Menzel, H. M. Woolf, and K. I. Strabala, 1994: Four Years of Global Cirrus Cloud Statistics Using HIRS. J. Clim., 7, 1972-1986.

and for cloud phase they are

Ackerman, S. A., W. L. Smith and H. E. Revercomb, 1990: The 27-28 October 1986 FIRE IFO cirrus case study: spectral properties of cirrus clouds in the 8-12 micron window. Mon. Wea. Rev., 118, 2377-2388.

Strabala, K. I., S. A. Ackerman and W. P. Menzel, 1994: Cloud properties inferred from 8-12 micron data. J. Appl. Meteor, 33, No. 2, 212-229.

2.0 Overview

Cirrus clouds are crucially important to global radiative processes and the heat balance of the Earth; they allow solar heating while reducing infrared radiation to space. Models of climate changes will have to correctly simulate these clouds to have the proper radiative terms for the Earth's heat budget. Past estimates of the variation of cloud cover and the Earth's outgoing longwave radiation have been derived primarily from the longwave infrared window (10-12 microns) radiances observed from polar orbiting and geostationary satellites (Rossow and Lacis, 1990; Gruber and Chen, 1988). The occurrence of semi-transparent clouds is often underestimated in these single channel approaches. Recently, multispectral techniques have been used to better detect cirrus in global (Wylie et al., 1994; Wu and Susskind, 1990) and North American (Wylie and Menzel, 1989) cloud studies.

Cloud phase also plays a role in regulating the Earth's energy budget; ice and water clouds react differently to similar incident radiation. For example, more absorption takes place in ice clouds between 10 and 12 microns than in water clouds of equal water content based on the indices of refraction. Therefore, changes in cloud phase will affect climate feedback mechanisms and must be included in global climate models. In the infrared window region, changes in microphysical properties from 8 to 11 microns and 11 to 12 microns allow three carefully chosen bands to differentiate cloud phase. Past infrared single band and bi-spectral split window cloud detection techniques (Booth, 1978; Inoue, 1987; Inoue, 1989) cannot fully take advantage of these properties; to date, no single operational satellite contains three bands within these spectral ranges. Visible channel cloud phase detection techniques exist (Pilewskie and Twomey, 1987; King, 1992), but do not provide complete temporal coverage.

MODIS offers the opportunity to investigate seasonal and annual changes in the cirrus or semi-transparent global cloud cover and cloud phase with multispectral observations at high spatial resolution (one km rather than the current operational 17 km). Transmissive clouds that are partially transparent to terrestrial radiation can be separated from opaque clouds in the

statistics of cloud cover (Wylie and Menzel, 1989). To date semi-transparent or cirrus clouds have been found in roughly 40% of all HIRS observations (Wylie et al., 1994).

3.0 Algorithm Description

The theoretical basis of the algorithms and practical considerations are contained in this section.

3.1 Theoretical Description

This section discusses the physics of deriving cloud height and amount, and cloud phase from multispectral infrared radiances from a given field of view, presents the application with MODIS data, and estimates different sources of error.

3.1.1.a Atmospheric Physics of Cloud Top Properties Algorithm

The CO_2 slicing technique is founded in the calculation of radiative transfer in an atmosphere with a single cloud layer. For a given cloud element in a field of view (FOV) the radiance observed, $R(\upsilon)$, in spectral band υ can be written

$$R(\upsilon) = (1 - NE)R_{clr}(\upsilon) + NE * R_{bcd}(\upsilon, P_c) \qquad (1)$$

where $R_{clr}(\upsilon)$ is the corresponding clear sky radiance, $R_{bcd}(\upsilon, P_c)$ is the corresponding radiance if the field of view were completely covered with an opaque or "black" cloud at pressure level P_c, N is the fraction of the field of view covered with cloud, and E is the cloud emissivity. It is apparent from this expression that for a given observed radiance, if the emissivity is overestimated, then the cloud top pressure is also overestimated (putting it too low in the atmosphere).

The opaque cloud radiance can be calculated

$$R_{bcd}(\upsilon, P_c) = R_{clr}(\upsilon) - \int_{P_c}^{P_s} \tau(\upsilon, p) \frac{dB[\upsilon, T(p)]}{dp} dp \qquad (2)$$

where P_s is the surface pressure, P_c is the cloud pressure, $\tau(\upsilon, p)$ is the fractional transmittance of radiation of frequency υ emitted from the atmospheric pressure level (p) arriving at the top of the atmosphere $(p = 0)$, and $B[\upsilon, T(p)]$ is the Planck radiance of frequency υ for temperature $T(p)$. The second term on the right represents the decrease in radiation from clear conditions introduced by the opaque cloud.

Following the work of Smith and Platt (1978) and Chahine (1974), to assign a cloud top pressure to a given cloud element, the ratio of the deviations in observed radiances, $R(\upsilon)$, and the corresponding clear air radiances, $R_{clr}(\upsilon)$, for two spectral channels of frequency υ_1 and υ_2 viewing the same FOV can be written as

$$\frac{R(\upsilon_1) - R_{clr}(\upsilon_1)}{R(\upsilon_2) - R_{clr}(\upsilon_2)} = \frac{NE_1 \int_{P_s}^{P_c} \tau(\upsilon_1, p) \frac{dB[\upsilon_1, T(p)]}{dp} dp}{NE_2 \int_{P_s}^{P_c} \tau(\upsilon_2, p) \frac{dB[\upsilon_2, T(p)]}{dp} dp} \qquad (3)$$

If the frequencies are close enough together, then E_1 approximates E_2, and one has an expression by which the pressure of the cloud within the FOV can be specified. The atmospheric temperature and transmittance profiles for the two spectral bands must be known or estimated.

Alternately, if clear sky radiances are unavailable, one can write a modified version of Equation (3) where the cloud top pressure is inferred from the radiance gradients in two CO2 slicing spectral bands within the area of interest (eg. 5 x 5 pixels).

$$\frac{R_{\min}(\upsilon_1) - R_{\max}(\upsilon_1)}{R_{\min}(\upsilon_2) - R_{\max}(\upsilon_2)} = \frac{(NE_{\min} - NE_{\max}) \int_{P_s}^{P_c} \tau(\upsilon_1, p) \frac{dB[\upsilon_1, T(p)]}{dp} dp}{(NE_{\min} - NE_{\max}) \int_{P_s}^{P_c} \tau(\upsilon_2, p) \frac{dB[\upsilon_2, T(p)]}{dp} dp} \qquad (3')$$

where $R_{\min}$ ($R_{\max}$) is the cloudiest (clearest) pixel and $NE_{\min}$ ($NE_{\max}$) is the associated effective emissivity. Similar to before, one assumes that the gradients in the effective emissivities for the clearest and cloudiest pixels in the two spectrally close channels are the same, and one can solve for the cloud top pressure of cloud. This mitigates the dependence on finding or forward calculating clear sky radiances (the former being prone to errors from undetected cloud and the latter suffering from radiance bias corrections). One assumes that the radiance gradients are due to changes in effective emissivity and not change in cloud top pressure.

Once a cloud height has been determined, an effective cloud amount (also referred to as effective emissivity) can be evaluated from the infrared window channel data using the relation

$$NE = \frac{R(w) - R_{clr}(w)}{B[w, T(P_c)] - R_{clr}(w)} \qquad (4)$$

Here N is the fractional cloud cover within the FOV, NE the effective cloud amount, w represents the window channel frequency, and $B[w, T(P_c)]$ is the opaque cloud radiance. Effective emissivity cannot be calculated without an estimate of the window channel clear sky radiance.

Effective emissivity refers to the product of the fractional cloud cover, N, and the cloud emissivity, E, for each observational area (5 x 5 pixels). When NE is less than unity, MODIS may be observing broken cloud $(N < 1, E = 1)$, overcast transmissive cloud $(N = 1, E < 1)$, or broken transmissive cloud $(N < 1, E < 1)$. With an observational area of roughly five kilometer resolution, the semi-transparency for a given field of view is more often due to cloud emissivity

being less than one than due to the cloud not completely covering the field of view; for most synoptic regimes, especially in the tropics and subtropics, this is found to be true (Wylie et al., 1994).

3.1.1.b Atmospheric Physics of Cloud Phase Algorithm

The tri-spectral technique also has its roots in the calculation of radiative transfer in the atmosphere. Single scattering processes can be parameterized in the cloud emissivity $E(\lambda)$ in Equation (1) (Parol et al., 1991). The single scattering properties are defined by the index of refraction, the cloud particle size distribution and the particle shape distribution. This section discusses the underlying physical principles that determine the capabilities and channel bandwidths of the proposed tri-spectral technique.

Absorption and emission by clouds are dependent upon the index of refraction of the cloud particles and their size. The index of refraction (m) of the particle is given by

$$m = n_r - n_i, \tag{5}$$

where n_r, the real portion, is an indication of the strength of scattering by the particle, and n_i, the complex portion, is an indication of absorptive properties of the material. Figure 1 depicts the real and imaginary portions of the index of refraction (after Warren, 1984) over the atmospheric window for both ice and liquid water. Differences in the values of the indices for water versus ice will result in distinctive reactions to similar incident radiation.

Minimum values of the imaginary portion of the index of refraction occur from 8-10 microns indicating weaker particle absorption. The ice and water indices increase and diverge beyond this spectral region. Cloud radiative properties are influenced by these particle characteristics. More absorption will take place in ice cloud between 10-12 microns than in water clouds of equal water content. This results in lower blackbody temperatures for ice than water

clouds of similar height, thickness, particle size, and water content. Ackerman et al. (1990), noted that blackbody temperature decreases with increasing wavelength for thick cirrus between wavelengths of 10 and 12 microns. This is consistent with the increase in the absorption coefficient,

$$\kappa(\lambda) = \frac{4\pi n_i}{\lambda} \tag{6}$$

whose shape closely resembles that of the imaginary index of refraction over this spectral interval.

Cloud radiative processes are also dependent upon the size of particles in the cloud. Model results indicate single scattering processes closely match the general shape of the indices of refraction for ice and water until reaching a size of 30 microns (Figure 2). Scattering processes are at a maximum from 8-9 microns and a minimum from 10.5-12 microns, however they are generally less important than absorptive properties in the window region. Cloud particle shape investigations revealed no significant differences in the spectral signature of the single scattering properties between ice spheres and infinite cylinders. Takano et al. (1992) showed similar results using spheriodal and hexagonal particles; scattering was greater at 8 microns then at 11 or 12 microns.

Atmospheric effects must also be accounted for in infrared cloud detection. In the absence of clouds, Equation (1) reverts to the standard clear sky form of the radiative transfer equation

$$R_{clr}(\lambda) = B(\lambda, T(p_s))\tau(\lambda, p_s) + \int_{P_s}^{P_0} B(\lambda, T(p))\frac{d\tau(\lambda, p)}{dp}dp \tag{7}$$

Scattering is negligible in the infrared region for a clear atmosphere since the wavelengths are much greater than the size of air molecules. As a result, differences in brightness temperature can be related to the amount of transmission of energy in each layer.

Total transmittances of a standard atmosphere were computed using FASCOD2 for the 8-13 micron spectral region using data gathered from the High-spectral resolution Interferometer Sounder (HIS) (Smith et al., 1991) and the resultant spectra is depicted in Figure 3. From 8 to 12 microns, the transmittance is generally greater than .7, with most of the absorption due to water vapor molecules. In a clear atmosphere over a surface with an emissivity of 1, the 8 minus 11 micron brightness temperature difference will be near zero or negative due to the stronger water vapor absorption that occurs at 8 than 11 microns.

Combining the results of atmospheric absorption with simulations of single scattering properties, regions of the infrared spectrum were selected that would be most useful for the detection of cloud.

In the 8-9 micron region, ice/water particle absorption is a minimum, while atmospheric water vapor absorption is moderate. In the 11-12 micron region, the opposite is true; particle absorption is maximum and atmospheric water vapor absorption is relatively small. Using bands in these two regions in tandem, cloud properties can be distinguished. Large positive brightness temperature differences in 8 minus 11 microns indicate the presence of cirrus clouds. This is due to the larger increase in the imaginary index of refraction of ice over that of water. For clear conditions, the 8 minus 11 micron brightness temperature difference will be small or even negative due to stronger atmospheric water vapor absorption at 8 microns than 11 microns. A third band in the 12 micron region will enable cloud phase delineation. Water particle absorption increases more between 11 and 12 microns then between 8 and 11 microns, while the increase of ice particle absorption is greater between 8 and 11 microns than between 11 and 12 microns. Thus, the 11 minus 12 micron brightness temperature differences of water clouds are greater than the 8 minus 11 micron differences. Conversely, 8 minus 11 micron brightness temperature differences of an ice cloud scene are greater than coincident 11 minus 12 micron differences. Therefore, ice and water clouds will separate in a scatter diagram of 8 minus 11 micron versus 11 minus 12 micron brightness temperature differences, with ice cloud scenes lying above the unity slope and

water clouds below. Mixed phase or partial radiometer filled ice over water clouds will exhibit characteristics of both ice and water clouds in this format, grouping near the unity slope.

3.1.2.a Mathematical Application of Cloud Top Properties Algorithm

The MODIS radiometer senses infrared radiation in seventeen spectral bands that lie between 3.75 and 14.24 microns at 1 km resolution (depending upon viewing angle) in addition to visible reflections at the same or better resolution. The four channels in the CO_2 absorption band (ch 33 at 13.34, ch 34 at 13.64, ch 35 at 13.94, and ch 36 at 14.24 microns) are used to differentiate cloud altitudes and the longwave infrared window channel (ch 31 at 11.03 microns) identifies the effective emissivity of the cloud in the MODIS field of view (FOV). Figure 4 indicates the weighting functions for the CO_2 absorption channels on MODIS.

Equation (3') will nominally be used to determine the mean cloud properties from a 5 x 5 FOV area; when single FOV cloud properties are desired Equation (3) must be used. The left side of Equation (3') is determined from the MODIS observed radiance gradients with the 5 x 5 FOV area (or for a single FOV, the MODIS measured radiances and the clear air radiances inferred from spatial analyses of nearby clear radiance observations). Equation (3') or (3) can only be solved for a portion of the atmosphere where there is a one to one relationship between temperature and pressure. The right side of Equation (3') or (3) is calculated from a temperature profile and the profiles of atmospheric transmittance for the spectral channels as a function of P_c, the cloud top pressure (the integration through the atmosphere is accomplished at discrete 50 mb intervals). It is anticipated that global analyses of temperature and moisture fields from the National Center of Environmental Prediction (NCEP) will be used to define the initial fields of temperature and moisture. Assuming that the emissivity of the clouds are the same for the two spectral channels, the desired solution is the P_c that best matches measured and calculated ratios; the search is restricted between the surface pressure (or the top of the inversion layer) and the tropopause.

Using the ratios of radiances of the four CO_2 spectral channels and the infrared window channel, five separate cloud top pressures can be determined (14.24/13.94, 13.94/13.64, 13.94/13.34, 13.64/13.34, and 13.34/11.03). Whenever $(R - R_{clr})$ or $(R_{\max} - R_{\min})$ is within the instrument noise (conservatively estimated at roughly .5 mW/m^2/ster/cm^{-1}), P_c cannot be determined reliably. Using the five cloud top pressures, as many as five effective cloud amount determinations can be made using Equation (4). As described by Menzel (1983), the most representative cloud height and amount are those that best satisfy the radiative transfer equation for the four CO_2 channels and the infrared window.

Once NE is determined, then E can be estimated. Using the cloud mask generated for all MODIS pixels (Ackerman et al., ATBD-MOD-06), an estimate of the cloud cover, N, for the 5 x 5 pixel array is made, and in turn E is inferred. The cloud top temperature is also readily estimated using a representative temperature profile (Menzel and Gumley, ATBD-MOD-07).

If no ratio of radiances can be reliably calculated because $(R - R_{clr})$ or $(R_{\max} - R_{\min})$ is within the instrument noise level, then a cloud top pressure is calculated directly from the infrared window channel (assuming it has adequate signal to noise). The MODIS observed 11.03 micron infrared window channel brightness temperature is compared with an in situ temperature profile to infer a cloud top pressure and the cloud cover, N, and the cloud emissivity, E, are assumed to be unity. In this way, all clouds are assigned a cloud top pressure either by CO_2 or infrared window calculations. Very thin high cloud are sometimes mistaken for low level opaque clouds; Wylie and Menzel (1989) found that this occurred for about half of the very thin clouds with NE less than 10%.

The calibrated and navigated MODIS data will be processed for 5 X 5 pixel areas. Fields of view are determined to be clear or cloudy from the cloud mask (Ackerman et al. ATBD-MOD-06). In the case where all 25 1 km FOV's are clear, no cloud parameters are calculated. The data also will be corrected for zenith angle, to minimize any problems caused by the increased path

length through the atmosphere of radiation upwelling to the satellite. Global coverage is expected every two days with one satellite. The algorithm is expected to be implemented as follows.

(1) From Equation (3′), the measured radiance gradients in the 5 x 5 pixel area for the CO2 slicing channels are used to determine the LHS (left hand side). A global model is used to calculate the RHS (right hand side) for a distribution of cloud top pressures; the forward calculated radiances must be adjusted for radiance bias (calculated - measured clear radiance) inferred for clear FOVs from previous month.

(2) For a given P_c, NE is calculated from measured longwave infrared window channel cloud forcing using Equation (4), where the clear radiance is the average of clear fovs within the 5 x 5 pixel area as designated by the cloud mask (if no clear FOVs, then check nearest neighbor boxes and borrow that value).

(3) P_c and NE are selected that best satisfy RTE for CO2 and IRW channels.

(4) Given NE, N is calculated by counting the number of cloudy FOVs in the cloud mask and dividing by 25; E is then inferred from NE/N.

(5) If radiance gradients or cloud forcing are too small (within instrument noise), infrared window channel solution for opaque cloud is used.

3.1.2.b Mathematical Application of Cloud Phase Algorithm

The essence of the tri-spectral method consists of interpreting a scatter diagram of 8 minus 11 micron versus 11 minus 12 micron brightness temperature differences, as from the 5 December 1991 MODIS Airborne Simulator (MAS) FIRE flight over the Gulf of Mexico (Figure 5). The 0.68 micron channel (with 50 m resolution) image is shown in Figure 6. The image is divided into smaller sub scenes according to cloud type, which are overlaid in color on the scatter diagram of Figure 5.

The clear region is identified by near zero or negative values of 8 minus 11 micron and small 11 minus 12 micron differences (Figure 6, scene 1). The magnitude of these differences depend upon the total column water vapor amount. Water and ice cloud separate in distinct

clusters with transmissive ice clouds grouped along a slope greater than one (Figure 6, scene 2) and water cloud less then one (Figure 6, scenes 4 and 5). Mixed phase cloud, or mixed cloud scenes, are identified by values in between, near the slope of unity (Figure 6, scene 6). Ice and water cloud with emissivities less than one are discerned by large positive values; large 8 minus 11 micron differences for ice cloud (Figure 6, scene 2 top pixels) and large 11 minus 12 micron differences for water cloud (Figure 6, scene 5). High emissivity cloud exhibit smaller values for both brightness temperature differences (Figure 6, scenes 3 and 4); most water vapor is trapped below an opaque cloud, creating a black cloud scene, where the same cloud temperature is sensed by all three channels.

The MODIS 8.55, 11.03 and 12.02 micron bands will be used to determine cloud phase over a 5 pixel x 5 pixel area. The MODIS cloud mask (MOD35) will be used to flag pixels which are clear. The brightness temperature for each band for a given FOV are averaged over each 5 by 5 pixel box. In turn, the standard deviation of the 8 micron radiance for each 5 x 5 pixel box is evaluated to determine scene uniformity over cloud scenes; which aids in opaque cloud determinations. The 8 micron channel is used with MAS data, however the 11 micron MODIS channel may be a better choice because it will also be evaluated for use with other techniques. A cluster analysis is applied to uniform cloudy scenes to differentiate opaque regions. A Maximum Likelihood Estimator (MLE) is then applied to all the averaged pixels for single phase delineation. Finally, multiphase areas are discerned on an averaged FOV by FOV basis, based solely on their location in the scatter diagram with respect to the unity slope. The 8 minus 11 micron versus 11 minus 12 micron scatter diagram will be made up of 2 along track and 270 cross track 5 x 5 pixel boxes (one instrument scan) for a total of ~540 data points. A step by step outline of the technique as applied to regions which were not flagged as entirely clear by the cloud mask follows.

1. Average the 8, 11 and 12 micron brightness temperatures over 5 x 5 pixel cloudy regions as determined by the cloud mask product (MOD35) for each scan (10 detector array).
2. Determine the 8 minus 11 micron and 11 minus 12 micron brightness temperature difference for each averaged pixel for the given scan.

3. Compute the standard deviation of the radiance for each cloudy 8 micron 5 x 5 pixel area per scan.

4. Apply a cluster analysis to averaged pixels within the scan that have an 8 micron radiance standard deviation less than .5 mW/ster/m^2/cm^{-1} as a means of differentiating opaque regions. The analysis utilizes the simple distance equation between two points for determining cluster centers,

$$dist = \sqrt{\Delta sd^2 + \Delta BT11^2}\ . \tag{8}$$

where sd refers to the standard deviation of the 8 micron radiance and BT11 is the 11 micron brightness temperature. Cluster "seeds" appear as the averaged pixels with the most number of points satisfying a distance tolerance of 1.0.

5. Determine the initial opaque cluster phase by checking the proximity of the cluster center to the unity slope in the brightness temperature difference scatter diagram. If the center lies above the unity slope on the 8 minus 11 versus 11 minus 12 micron brightness temperature difference the entire cluster is labeled as an opaque ice cloud; if below it is labeled an opaque water cloud. The center can also be identified if the 11 micron brightness temperature is less than 230 K (ice) or greater than 275 K (water).

6. Apply a maximum likelihood estimator to all averaged pixels with an 11 micron brightness temperature greater than 255 K,

$$\chi^2 = \left(\frac{1}{\sigma_x^2 + \sigma_y^2}\right)\sum_{i=1}^{N}\frac{\left(y_i - mx_i - b\right)^2}{\left(1 - m^2\right)}\ . \tag{9}$$

This provides an indication of the quality of a linear fit to the data (y versus x) given errors in both directions. Here σ_x^2 and σ_y^2 are the errors in both the x (11 minus 12 micron brightness temperature difference) and y (8 minus 11 micron brightness temperature difference) directions (.30 K and .35 K respectively for the MAS instrument TOGA/COARE deployment), b is the intercept and m is the slope. If a Gamma fit to the data is good (=1.00) and the χ^2 value is less than the number of averaged pixels, then the slope is tested for single phase clouds. If the slope is greater than 1, then the scene is labeled as a single phase ice cloud, if the slope is less than one, it

is a single phase water cloud. This overrides any phase determinations made in the cluster identification. For MODIS data implementation, the errors in both directions should be considerably lower. The specifications for the three infrared channels call for $NE\Delta T$'s of 0.05 K. 7. If a good fit is not found, a multi-phase cloud region is assumed. From here, each unclustered averaged FOV is tested for its' proximity to the unity slope. If the FOV lies within .3 K of the unity slope it is flagged as a mixed scene. If the 8 minus 11 micron versus 11 minus 12 micron brightness temperature lies above the unity slope, it will be labeled a non-opaque ice cloud, below a non-opaque water cloud. Points which fall within .3 K of the unity slope are labeled as mixed phase clouds.

Figure 7 is an example of an 8 minus 11 micron versus 11 minus 12 micron brightness temperature difference scatter diagram from two distinctly different cloud scenes; a water cloud scene from 18 January 1993 MAS TOGA/COARE data collected over the western Pacific and an ice cloud scene collected 16 April 1996 over Oklahoma during the SUbsonic aircraft: Contrail and Cloud Effects Special Study (SUCCESS) field campaign. The MLE statistics for the two scenes are included. The resultant phase determination for the ice cloud scene is overlaid on the MAS 11 micron imagery in Figure 8; also included is the Cloud Lidar System (CLS) (Spinhirne, 1990) data for the same time. It flies onboard NASA's ER-2 and corroborates the presence of a cirrus cloud with tops at 11.5 km during this time.

3.1.3.a Estimate of Errors of Cloud Top Properties Algorithm

In the study of Wylie and Menzel (1989), the CO_2 cloud heights derived from VAS (VISSR Atmospheric Sounder) data over North America were found to be of good quality when compared to three other independent sources of cloud height information. Results showed: (a) for about thirty different clouds, the CO_2 heights were within 40 mb rms of cloud heights inferred from radiosonde moisture profiles; (b) in 100 comparisons with lidar scans of clouds, the CO_2 heights were 70 mb lower on the average and were within 80 mb rms; (c) satellite stereo parallax measurements in 100 clouds compared to within 40 mb rms. The CO_2 heights appeared to be consistent with other measurements within 50 mb and the effective fractional cloud cover within

0.20 in most cloud types. The CO_2 slicing technique works best for middle and high clouds, but has trouble with very low clouds.

3.1.3.a.1 Errors Associated with the Assumption of Constant Emissivity

Spectrally close channels are used to minimize differences in the cloud emissivity between the two spectral channels. Calculations by Jacobowitz (1970) indicate that negligible error occurs in the cloud top pressure estimation using the assumption of constant emissivity for the CO_2 channels between 13.3 and 14.2 microns.

3.1.3.a.2 Errors Associated with the Assumption of a Thin Cloud Layer

The CO_2 slicing algorithm assumes that all of the radiative effects of the cloud occur in the top thin layer. This makes the mathematics tractable. If the radiative transfer integral of Equation (3) were to include a cloud term where the cloud has finite depth, then a knowledge of the vertical structure of the cloud would be required. There are an infinite variety of combinations of cloud depths and vertical combinations that could produce the same integrated radiative signature; a unique solution is not possible. Any initial assumption of cloud structure biases the cloud top and bottom solution derived in the radiative transfer formulation.

The thin layer cloud approximation is investigated in Smith and Platt (1978). They found that errors in the height assignment approaching one-half (one-quarter) the thickness of the cloud were introduced for optically thin (thick) clouds where the integrated emissivity is less than (greater than) .6. The largest errors will be associated with physically thick but optically thin cirrus clouds. For optically thin (very transparent) cirrus with 100 mb depth the error in the height estimate is roughly 50 mb.

Wielicki and Coakley (1981) also discussed the consequences of the thin layer cloud approximation. They concluded that the algorithm solution (P_c) would be near the center of the cloud for optically thin clouds and near the top of the cloud for optically thick clouds. This is

similar to a center of mass concept. The algorithm solution will thus be close to the "radiative center" of the cloud. Thus, P_c is somewhere between the cloud top and its center varying with the density of the cloud.

Cirrus height errors are also discussed in Wylie and Menzel (1989) where VAS cloud top pressure estimates were compared to cloud tops measured by lidars and by the stereo parallax observed from the images of two satellites at two different viewing angles. VAS CO_2 channels (14.25, 14.01, and 13.33 microns) are similar to three of the four on MODIS. In the lidar comparison, the VAS inferred cloud top pressure over an observation area was compared to the highest lidar observation in the same area; these clouds had to be radiatively thin for the lidars to see through to the tops. Definition of a single cloud top was often difficult within a cloud layer; the lidar heights varied considerably (by more than 50 mb) from one cloud element to another in the same cloud layer. On the average, the VAS P_c was found to be 70 mb larger (lower cloud altitude) than the tops seen on the lidars. The CO_2 slicing technique was sensing the mean height; the VAS heights were comparable to the lidar top heights to within half the cloud thickness. In the comparisons to stereo parallax measurements for thin transmissive clouds, the VAS heights showed little bias. It was often difficult to measure parallax for thin transmissive clouds, as they appeared fuzzy with poorly defined boundaries in the images. Since the image of the clouds is more indicative of the center of the diffuse cloud mass than its outer boundaries, the parallax method is also sensitive to the radiative center of mass rather than the physical tops of these clouds. Thus, in these intercomparisons of actual measurements, the CO_2 cloud top pressures were found to be within the accuracy suggested by theoretical considerations.

3.1.3.a.3 Errors Associated with the Presence of a Lower Cloud Layer

The algorithm assumes that there is only one cloud layer. However, for over 50% of satellite reports of upper tropospheric opaque cloud, the ground observer indicates additional cloud layers below (Menzel and Strabala, 1989). To understand the effects of lower cloud layers, consider the radiation sensed in a cloudy field of view. For a semi-transparent or cirrus cloud layer, the radiation reaching the satellite, R, is given by

$$R = R_a + E * R_c + (1 - E) * R_b \tag{10}$$

where R_a is the radiation coming from above the cloud, R_c is the radiation coming from the cloud itself, R_b is the radiation coming from below the cloud, and E is the cloud emissivity. When a lower cloud layer is present under the semi-transparent or cirrus cloud, R_b is smaller (i.e., some of the warmer surface is obscured by the colder cloud). If prime indicates a two layer cloud situation of high semi-transparent cloud over lower cloud, and no prime indicates a single layer high semi-transparent cloud, then

$$R_b' < R_b, \tag{11}$$

which implies

$$R' < R. \tag{12}$$

Thus the difference of cloud and clear radiance is greater for the two layer situation,

$$[R_{clr} - R'] > [R_{clr} - R]. \tag{13}$$

The effect of two cloud layers is greater for the 13.3 micron channel than for the other CO_2 micron channels, because the 13.3 micron channel "sees" lower into the atmosphere (Figure 4 shows the weighting functions where the 13.3 peaks lower in the atmosphere than the other CO_2 channels). So using the 13.9/13.3 ratio as an example

$$[R_{clr}(13.3) - R'(13.3)] > [R_{clr}(13.9) - R'(13.9)]. \tag{14}$$

This reduces the ratio of the clear minus cloud radiance deviation in Equation (3) because the denominator is affected more than the numerator (when the less transmissive channel is in the numerator),

$$\frac{\left[R_{clr}(13.9) - R'(13.9)\right]}{\left[R_{clr}(13.3) - R'(13.3)\right]} < \frac{\left[R_{clr}(13.9) - R(13.9)\right]}{\left[R_{clr}(13.3) - R(13.3)\right]}, \tag{15}$$

or Left' < Left, where Left refers to the left side of Equation (3). An example plot of P_c versus Right (where Right refers to the right side of Equation (3)), shown in Figure 9, indicates that Left' < Left implies $P_c' > P_c$. Thus, when calculating a cloud pressure for the upper semi-transparent cloud layer in a two cloud layer situation, the CO_2 slicing algorithm places the upper cloud layer too low in the atmosphere.

An example from 25 October 1990 using VISSR Atmospheric Sounder (VAS) data is presented to illustrate further the magnitude of the errors that can be induced by lower level clouds (results for other days and other situations were found to be comparable). Ground observers in Omaha, Nebraska reported thin cirrus clouds with no other underlying clouds present. The ratio of the 13.9 to 13.3 micron satellite observed radiance differences between clear and cloudy FOVs (the left side of Equation (3)) is 0.36 on 25 October. This implies single layer cloud at 300 mb (solving the right side of Equation (3) for P_c as shown in Figure 9).

R' has been modeled for a semi-transparent cloud at 300 mb with an underlying opaque cloud layer at 920, 780, 670, 500, and 400 mb (each configuration produces a different ratio in the left side of Equation (3), Left'). The different Left' suggest different P_c' solutions as Left' is matched to Right, the right side of Equation (3). In the absence of any knowledge of a lower layer, the CO_2 algorithm integrates the right side of Equation (3) from the surface to an incorrect P_c'. Figure 9 shows Right as a function of P_c for the situation of 25 October. The errors in

calculated cloud top pressure from the original 300 mb solution, $P_c' - P_c$, are shown as a function of height of the underlying opaque cloud layer in Figure 10a for 25 October.

In the two cloud layer situation, the position of the lower cloud layer affects the accuracy of the estimate of the height of the upper cloud layer. Opaque clouds in the lower troposphere underneath high cirrus have little affect on the cirrus P_c. Inspection of the spectral transmittance show that neither the 14.2 or the 13.9 micron channels are very sensitive to radiation from low in the troposphere, while the 13.3 micron channel senses only about half of the radiation from below 800 mb. Opaque clouds in the middle troposphere, between 400 and 800 mb, underneath high cirrus, cause the cirrus P_c to be overestimated (lower in the atmosphere) by up to 220 mb (this extreme occurs for the very thin high cirrus cloud with NE of 0.10). The decreases in R_b produce smaller ratios for the left side of Equation (3) which in turn produces larger estimates of P_c. Opaque clouds high in the atmosphere, underneath higher cirrus, have little effect on the cirrus P_c, since the height of the lower opaque layer approaches the height of the semi-transparent upper cloud layer and the CO_2 algorithm is going to estimate a height in between the two layers.

The errors in P_c were also examined for different emissivities of transmissive clouds (see Figure 10b). This was modeled by varying the emissivity and forming new ratios on the left side of Equation (3). The maximum cloud top pressure error of roughly 220 mb occurred in very thin cloud with emissivity of 0.10. The error in P_c reduced as the emissivity of the transmissive clouds increased. For a cloud with emissivity of 0.5, the maximum error in P_c is about 100 mb. For more dense clouds with emissivity of 0.9, the maximum error in P_c is less than 20 mb. The VAS data have shown a nearly uniform population of emissivity center around 0.5 (Wylie and Menzel, 1989), so one can conclude that the errors in the cloud top pressure caused by underlying clouds should average under 100 mb.

Multi-layer cloud situations (transmissive over opaque cloud) cause the height estimate of the upper cloud to be about 100 mb too low in the atmosphere on the average. The error in

transmissive cloud height is largest when the underlying opaque layer is in the middle troposphere (400- 700 mb) and small to negligible when the opaque layer is near the surface or close to the transmissive layer. The error in effective emissivity increases as the opaque layer approaches the transmissive layer; when they are coincident, the effective emissivity is assumed to be one. In summary the cloud forcing from two layers is greater than the cloud forcing from one layer; assuming only one cloud layer when two exist causes the CO_2 solution to put the cloud between the two layers with larger effective emissivity. This suggests that, overall, global cloud parameter estimates will be a little low in the atmosphere and with an effective emissivity a little too high.

Recent work has suggested that the radiative transfer equation in a two layer cloud situation can be solved from the CO_2 radiance observations. The two layer cloud forcing can be written, where u is the upper cloud layer and l is the lower cloud layer,

$$R - R_{clr} = N_l E_l \left[1 - N_u E_u\right] \int_{P_s}^{P_{cl}} \tau dB + N_u E_u \int_{P_s}^{P_{cu}} \tau dB \qquad (16)$$

Thus the two layer cloud forcing is characterized by four unknowns $N_l E_l$, $N_u E_u$, P_{cl}, and P_{cu}. Using the measured cloud forcing in the CO_2 channels, a solution for upper and lower cloud pressures and effective cloud amounts is calculated. The algorithm selects spectrally close pairs of CO_2 channels. For each pair of cloud forcing measurements, all possible $N_l E_l$, $N_u E_u$ are calculated as a function of P_{cl}, P_{cu}. From this array of possible solutions, the selected solution best satisfies the radiative transfer equation for all spectral channels. Since four unknowns offer more degrees of freedom than two unknowns, the two layer solution is preferred over the one layer solution. Indication of when to use the two layer solution is sought through inspection of 4.0 micron versus 11.0 micron radiance scatter plots for the 5 x 5 pixel area (when radiances for the two spectral channels lie on two or more straight lines then the presence of two or more cloud layers is suggested). More development work remains, before the two layer solution can be incorporated into the cloud parameter algorithm.

3.1.3.a.4 Errors from an Inaccurate Estimate of the Surface Temperature

The CO_2 slicing algorithm has little sensitivity to surface temperature. The weighting functions for the CO_2 channels indicate that very little radiation from the Earth surface is detected by the satellite radiometer in these spectral bands (14.2 and 13.9 micron observations don't even see the ground). Table 1 indicates the changes in cloud top pressure associated with changes in estimates of surface temperature inferred from a recalculation of the right side of Equation (3); the atmospheric profile of 25 October was used as an example (other situations yield similar results). When the surface temperature T_{sfc} is assumed to be 5 C too warm, the cloud top pressure P_c is 32 mb smaller (higher in the atmosphere); when T_{sfc} is assumed to be 5 C too cold, P_c is 26 mb larger (lower in the atmosphere). In other words, when the surface temperature guess doesn't track surface warming (cooling), then the cloud layer is calculated to be too low (high).

Table 1. The changes in cloud top pressures (P_c) and effective emissivities determined from the CO_2 slicing algorithm after changes to the estimated temperature profile and surface temperature (using the data of 25 October 1990).

	Guess Error (guess - truth)		Cloud Top Pressure and Effective Emissivity Error					
					with additional errors from faulty cloud screening for contaminating clouds at			
					300mb		700mb	
met cond	sfc DTs	atm $DT_{(p)}$	DP_c	$D(NE)$	DP_c	$D(NE)$	DP_c	$D(NE)$
a	+5 K	0 K	-32 mb	-.09				
b	-5	0	+26	+.13	+39 mb	+.13	+20 mb	+.09
d	0	+2	+10	+.03				
c	0	-2	-13	-.03				
ad	+5	+2	-20	-.07				
ac	+5	-2	-44	-.11				
bd	-5	+2	+37	+.19	+50	+.19	+31	+.14
bc	-5	2	+16	+.09	+28	+.09	+09	+.06

Possible meteorological conditions that could cause indicated errors in the guess

a indicates nocturnal cooling
b indicates solar heating
c indicates warm frontal passage
d indicates cold frontal passage

Table 1 also indicates an additional effect that arises when the surface temperature is assumed to be too cold. In the cloud screening process, some cloudy FOVs are inferred to be clear and R_{clr} is reduced for all spectral channels. Thus the left side of Equation (3) is reduced (when the less transmissive channel is in the numerator) and P_c goes even larger (lower in the atmosphere). The last four columns of Table 1 show the total error when 25% of the FOVs are incorrectly inferred to be clear for a guess that is 5 C too cold; when high clouds at 300 mb contaminate the clear radiance determination, P_c is 39 mb larger (representing an additional error of 13 mb), and when low clouds at 700 mb contaminate the clear radiance determination, P_c is 20 mb larger (representing an offsetting error of 6 mb).

The surface temperatures are monitored hourly with the SVCA conventional observations; errors of 5 C are unusual, but do occur in the western mountains where surface observations are too sparse to accurately represent the varying altitude conditions. We conclude that nominal diurnal changes in surface temperature will not affect the CO_2 slicing solutions of P_c by more than 50 mb.

Furthermore, fictitious reports of transmissive clouds cannot be produced by changes in the ground surface temperature, since two of the three channels do not see the ground. As witnessed in Table 1, effective emissivity estimates are relatively insensitive to surface temperature excursions of 5 C; NE changes of about 0.10 are found.

The preceding discussion also implies that the CO2 algorithm is insensitive to surface emissivity changes since 5% changes in surface temperature can be equated with roughly 7% changes in surface emissivity for the long wavelength channels.

3.1.3.a.5 Errors from an Inaccurate Estimate of the Temperature Profile

Table 1 also shows the changes in cloud top pressure associated with changes in estimates of temperature profile as well as surface temperature for the example of 25 October. When the entire temperature profile was changed by +/- 2 K in the calculation of the right side of Equation (3), the resulting changes were very small; about 10 mb for P_c and 0.03 for NE. These errors are roughly inversely proportional to the lapse rate at the altitude of the cloud. When the surface temperature and the atmospheric temperature were adjusted by 5 and 2 K respectively, maximum errors of roughly 40 mb in P_c and 0.20 in NE were found for the situation where the surface temperature was underestimated and the atmospheric temperature was overestimated (perhaps possible in nearly clear sky with strong solar heating producing a very large lapse rate in the lower atmosphere). Where the surface temperature and the atmospheric temperature were both underestimated (possible in a warm frontal passage), the cloud was estimated to be too low in the atmosphere by 20 mb in P_c and too opaque by 0.10 in NE.

Experiments were also conducted simulating errors localized to only one level of the temperature profile. The results (not shown) were modified minimally. Little sensitivity is apparent for temperature errors low in the atmosphere ($P_c > 700$), as expected from inspecting the transmittances of the MODIS CO_2 channels. An error of 2 C for a level between 700 and 300 mb can produce a shift of up to 30 mb in the cloud top pressure. This should be viewed in conjunction with the lapse rate of 5 C per 50 mb for the example of 25 October. Here and in other situations inspected, the errors in the CO_2 slicing cloud top pressure estimate, DP_c, caused by sounding errors, DT, in layers where the CO_2 spectral channels have sensitivity, are found to be roughly inversely proportional to the lapse rate at the level of the cloud, L; this can be expressed as $DP_C = DT/L$.

3.1.3.a.6 Errors Associated with Instrument Noise

The VAS radiometer is accurate to better than 1 mW/m2/ster/cm_1. This corresponds to less than 1 K in the CO_2 channels for temperatures ranging from 220 to 320 K. Noise affects the ability of the VAS to detect thin cirrus. Noise of 1 K implies that effective cloud emissivities of less than 10% cannot be resolved for high clouds (using $D(NE) = DR/(R - R_{clr})$. In our earlier work of 1989, it was found that about half of the very thin clouds with NE less than 0.10 were classified incorrectly as low opaque cloud observations (this represented about 5% of all observations); it was also found that about half of these very thin clouds were correctly classified by the CO_2 slicing algorithm.

The CO_2 slicing technique cannot measure the properties of clouds where the contrast of radiation from cloud free and cloud obscured observations is too small for reliable discrimination in the satellite CO_2 spectral radiances (when radiance differences are less than .5 $mW/m^2/ster/cm^{-1}$ cloud properties are not calculated). This occurs for very thin cirrus (as discussed in the previous paragraph) and for some low clouds below 700 mb. Clouds below 700 mb were assumed to have an effective emissivity of one, thus preventing the interpretation of low broken cloud as cirrus. Occasionally, low clouds were also reported in situations of clear sky with tropospheric temperature inversions; this created problems in early morning statistics during the winter months.

When noise is introduced in one channel of the CO_2 radiance ratio, the left side of Equation (3) changes. Using the example of 25 October once again, Figure 9 shows the noise induced changes in the ratio. The extremes produce a P_c that is 50 mb lower or make it impossible to have a solution in the atmosphere. This example is representative of further noise investigations in the CO_2 slicing algorithm; the effect of sensor noise is typically less than 50 mb.

3.1.3.a.7 Conclusions of the Cloud Top Pressure and Emissivity Error Studies

(i) Errors associated with the assumption of constant emissivity for the CO_2 channels are negligible.

(ii) The CO_2 slicing algorithm determines the height of the radiative center of the cloud; for optically thick clouds this is near the cloud top while for optically thin clouds it is near the cloud middle.

(iii) Multi-layer cloud situations where an opaque cloud underlies a transmissive cloud cause errors in the height of the transmissive cloud of about 100 mb for most cases (the cloud is determined to be too low in the atmosphere). The error in transmissive cloud height is largest when the underlying opaque layer is in the middle troposphere (400- 700 mb) and small to negligible when the opaque layer is near the surface or close to the transmissive layer.

(iv) When the surface temperature guess doesn't track surface warming (cooling), then the cloud layer is calculated to be too low (high). Nominal diurnal changes in the ground temperature are typically tracked to better than 5 C in the CO_2 slicing algorithm, so that they have little effect on the ability to detect transmissive clouds or to determine their heights.

(v) The CO_2 solution is largely insensitive to errors in the temperature sounding in the lower troposphere. There are often compensating effects in the integration of the atmospheric column. The errors in the CO_2 slicing cloud top pressure estimate caused by sounding errors in layers where the CO_2 spectral channels have sensitivity are roughly inversely proportional to the lapse rate at the level of the cloud.

(vi) Instrument noise causes the CO_2 slicing algorithm to miss roughly half of the thin cirrus with effective emissivity less than 0.10; this represents about 5% of all observations.

3.1.3.b Error Estimates of Cloud Phase Algorithm

Modeled results and observations of the infrared cloud phase determination suggest it is very reliable in the determination of single level, single phase clouds. Verification of cloud phase has been made through coincident lidar comparisons (Ackerman et al, 1990) and through

comparisons with a visible channel technique (Strabala et al. 1994). Known sources of error are discussed below.

3.1.3.b.1 Errors Due to Mixed Phase Cloud Scenes

Errors in cloud phase determination will take place due to overlap in the location of mixed phase and mixed level clouds in the 8 minus 11 versus 11 minus 12 micron brightness temperature difference scatter diagram. This ambiguity can be seen in the multi-phase cloud example of Figure 5. Notice the overlap between the thin cirrus over water cloud type and other cloud regimes. Cloud phase identification may error for mixed layer and mixed phase scenes, especially for very low emissivity cloud, where the signal is very close to that of clear sky.

3.1.3.b.2 Errors Due to Non-uniform Surface Emissivities

The current version of the tri-spectral technique assumes a uniform surface emissivity for all three channels. This is certainly not the case for many different ground surface types, including bare soils and deserts. Gao and Wiscombe 1994 modeled the effects of different surface types on the 8 minus 11 and 11 minus 12 micron brightness temperature differences based on laboratory surface emissivity measurements. Their results suggest that certain types of bare rock, and dry vegetation will lead to misidentification of cloud phase by the tri-spectral technique due the resultant location of the brightness temperatures differences on the scatter diagram. Many different MAS data sets over numerous surface types have been investigated to date; this includes recent SUCCESS overflights of bare Oklahoma riverbanks and high Utah desert. These affect the 8 micron band the most, and lead to large negative 8 minus 11 micron brightness temperature differences. This has the opposite effect as that of cloud, and should not interfere with cloud phase identification.

3.1.3.b.3 Errors Due to Instrument Noise

An investigation into the effects of MAS pixel averaging on brightness temperature differencing was conducted, with distinct cloud signals becoming apparent after averaging over a 5 x 5 pixel box. This lowers the NEDT values for the 8, 11 and 12 micron channels (as evaluated for MAS 5 December 1993 data) to 0.13, 0.09 and 0.15 K respectively. The MODIS NEDT specifications of these infrared bands at 300 K is 0.05 K, suggesting that the noise will be within the limits for cloud phase delineation.

3.2 Practical Considerations

3.2.1.a Radiance Biases and Numerical Considerations of Cloud Top Properties Algorithm

The MODIS measured radiances will have biases with respect to the forward calculated radiances using model estimates of the temperature and moisture profile for a given field of view. There are several possible causes for this bias: these include calibration errors, spectral response uncertainty, undetected cloud in the FOV, and model uncertainty. Solution of Equation (3) and (4) uses measured and calculated cloud forcing (clear minus cloudy FOV radiances) and thus requires that this bias be minimized. Techniques developed at the European Centre for Medium range Weather Forecast to characterize the HIRS radiance bias with respect to the ECMWF model (Eyre, 1992) will be employed in the MODIS cloud algorithm.

The measured and the calculated radiance gradient ratios in Equation (3) or (3') do not always converge within the allowable pressure bounds (between the tropopause and the top of the inversion layer or the surface). Solutions are not accepted if found at the boundaries, even though there may be a good meteorological reason to accept these values. In these cases the opaque cloud solution from the window channel is used.

Evaluation of the integrals in the right side of Equation (3) or (3') are performed at 50 mb increments. When the slope in Figure 9 increases, instrument noise causes more error in the cloud

top pressure determination. It has been found that mid-latitudes have greater slopes than the topics, thus cloud top pressures in the tropics might be slightly less error prone.

3.2.1.b Numerical Considerations of Cloud Phase Algorithm

The simplicity of the cloud phase algorithm, which relies on relatively simple mathematics, make it numerically stable. Post launch adjustments may be made initially to fine tune the SD and slope thresholds, due to band differences between the MAS and MODIS instruments.

3.2.2.a Programming Considerations of Cloud Top Properties Algorithm

Processing will be accomplished for every 5 x 5 pixel area (5 km resolution at nadir). The clear sky radiances come from a spatial analyses of the pixels designated clear by the cloud mask. Spatial registration of the channels must occur, so that FOVs can be collocated with ancillary data.

The CO_2 slicing algorithm has been used for the past nine years on VAS data over North America and for the past seven years on global HIRS data. It is a robust algorithm. The census of cirrus clouds derived from both of these efforts has been published in refereed literature.

The MODIS Level 2 cloud top properties algorithm has been run using simulated MODIS and actual HIRS radiances on the GSFC TLCF (SGI) for a MODIS granule (2.5 minutes or 100 scans). Several steps were taken to come to a final volume and load estimate. Timing runs were made on the TLCF SGI Power Challenge (modispc) using UNIX /bin/time command on a completely cloudy input granule (a synthetic granule with all pixels containing an identical set of cloudy HIRS radiances). We assumed in practice that only half of the 5x5 boxes viewed would actually contain a sufficient number of the cloudy pixels to be able to process. The processing rate on modispc was set at 93.75 Million Floating Point Operations per Second (MFLOPS), but divided by a factor of 4, which is the ECS average fraction of peak used by a process. The number of Million Floating Point Operations (MFPO) was then multiplied by 1.6 to factor in

additional processing needed in a production environment. The production code was timed at 408s per granule.

MFPO/granule = 1.6*0.5 cloud 5x5 pixels *(93.75/4 MFLOPS)*408s = 7650 MFPO/granule.

MFLOPS = (7650 MFPO/granule * 585.5 granules/day)/86400 s/day = 51.8 MFLOPS

The product Level 2 volume per granule is 5.4MB. A full day of MODIS processing will then result in a volume load of 5.4MB/granule * 585.5 granules/day = 3.2 GB/day for the first 51 parameters listed in Table 5.

3.2.2.b Programming Considerations for Cloud Phase Algorithm

Processing will be accomplished globally at 5 x 5 pixel resolution. The brightness temperatures will be averaged and cloud phase will be determined from a scatter diagram of ~540 averaged pixels. Spectral channel registration must occur before, so that FOVs can be collocated with ancillary data.

The cloud phase algorithm timing was estimated with the same assumptions used for the cloud top properties algorithm timing. It was timed at 61s per granule.

MFPO/granule = 1.6*0.5 cloud 5x5 pixels *(93.75/4 MFLOPS)*61s = 1143 MFPO/granule.

MFLOPS = (1143 MFPO/granule * 585.5 granules/day)/86400 s/day = 7.7 MFLOPS

The product Level 2 volume per granule is .7MB. A full day of MODIS processing will then result in a volume load of .7/granule * 585.5 granules/day = 410 MB/day for the parameters 52-58 listed in Table 5.

3.2.3. Validation

Validation will be approached in several ways: (i) collocation with higher resolution aircraft data, (ii) ground-based and aircraft in situ observations, and (iii) intercomparisons with other AM-1 platform instruments. Our validation approach relies heavily on the sources of the data that were used in the algorithm development, which consisted primarily of the MAS, a fifty channel visible, near-infrared, and thermal infrared imaging spectrometer with 50 m resolution at nadir (cf. King et al. 1996), HIS, a 2 km resolution nadir-viewing Michelson interferometer with 0.5 cm^{-1} spectral resolution from 4 to 15 μm (Revercomb et al. 1988), and AVIRIS, a 224 band imaging spectrometer from 0.4-2.5 μm with 20 m resolution at nadir.

Well-calibrated radiances are essential for the development of accurate algorithms. The calibration of the HIS is such that it serves as a reference for line-by-line radiative transfer models. The MAS infrared channels are calibrated through two onboard blackbody sources that are viewed once every scan. Calibration of the shortwave infrared and thermal infrared channels will be routinely assessed through vicarious calibration and intercomparisons with the HIS flying on the same aircraft. The MAS solar channels are calibrated in the field, using a 30" integrating sphere before and after each ER-2 deployment, as well as a 20" integrating hemisphere shipped to the field deployment site for periodic calibrations during a mission. A comprehensive description of both the shortwave and longwave calibration procedures, signal-to-noise characteristics, and thermal vacuum characterization of the MAS can be found in King et al. (1996).

Several field campaigns are planned with the ER-2 aircraft carrying the MAS and HIS over various scenes and ecosystems. In addition to the major national and international activities outlined above, we envision the following focused and short field deployments:

- winter deployment over the Great Lakes, Hudson Bay, sea ice, and lake ice (based in Madison, WI);
- summer deployment over the ocean, mountains, and desert (based in Mountain View, CA).

A ground campaign with the ER-2 over the Atmospheric Radiation Measurement (ARM) CART (Clouds And Radiation Testbed) site in Oklahoma would entail:

- post-launch deployment of the MAS and HIS on the ER-2 aircraft to coincide with a MODIS overflight and to collect simultaneous ground-based class-sondes, AERI (a ground-based Michelson interferometer), tower measurements of temperature and moisture at various elevations, microwave moisture measurements, lidar and radar cloud observations, and whole sky camera images.

A ground campaign with all sky cameras (from the University of Chicago, Dr. Ted Fujita) would coincide with

- winter and summer in the upper Midwest.

Comparisons with products from other platforms are also planned. Cloud masks will be compared with those from AVHRR and HIRS/2 data, ASTER and MISR (also on the AM-1 platform), and CERES. Atmospheric profiles will be compared with those from HIRS, GOES, and AIRS (also on the PM-1 platform). Cloud properties will be intercompared with those derived from HIRS, GOES, CERES, MISR and AIRS, as well as from in situ aircraft (see below). Timing, coverage and resolution will vary from one instrument to another; for example with ASTER, comparisons will be possible for selected swaths (60 km wide with 30 m resolution) that are available for different (and selected) ecosystems no more than once every 16 days.

Table 2. MODIS Field Campaigns to be used in Cloud Properties Validation

Mission	***Dates***	***Responsible Team Members***	***Primary Purpose***
SUCCESS	April-May 1996	Si-Chee Tsay, Steve Ackerman, Steve Platnick	cirrus cloud properties with MAS and HIS
WINCE	February 1997	Paul Menzel, Steve Ackerman, Dorothy Hall	cloud detection and properties over snow/ice covered land and lakes

			with MAS and HIS
FIRE III	April-June 1998 August 1998	Michael King Si-Chee Tsay	arctic stratus clouds over sea ice
ARM-1	August- September 1998	Paul Menzel, Steve Ackerman, Dan LaPorte,Bill Smith	periodic flights over the Oklahoma ARM site with MAS & HIS & NAST
MOBY	December 1998	Paul Menzel, Steve Ackerman	cirrus clouds and atmospheric corrections over the ocean with MAS and NAST
ARM-2	April-May 1999	Paul Menzel, Steve Ackerman, Dan LaPorte,Bill Smith	periodic flights over the Oklahoma ARM site with MAS & HIS & NAST
LBA	September 1999	?	tropical clouds and biomass burning
California	July 1999 December 1999	Michael King, Steve Platnick, Si-Chee Tsay	marine stratocumulus and valley fog

Several field programs offer opportunities for pre-launch and post-launch MODIS validation through collection and analysis of observations obtained from the MODIS Airborne Simulator (MAS; King et al. 1996) and High-spectral resolution Interferometer Sounder (HIS; Revercomb et al. 1988). Those field campaigns relating primarily to cloud top properties and cloud phase are found in Table 2.

The Subsonic Aircraft Contrail and Cloud Effects Special Study (SUCCESS) field experiment in April-May 1996 had the goal of determining the radiative properties of cirrus contrails, and to contrast them with naturally occurring cirrus. To assess the radiative impact of these clouds requires a well-calibrated set of radiation measurements and "ground (or in situ) truth" observations. During SUCCESS several MAS and HIS multispectral observations from the NASA ER-2 aircraft were coordinated with in situ aircraft and ground based measurements. The MAS and HIS measurements address the very important relationship between cirrus radiative properties and the thermodynamic environment (atmospheric temperature and moisture conditions) wherein cirrus clouds form and are maintained. The HIS provides accurate measurements of the atmospheric thermodynamical properties supporting the cirrus life cycle and

the MAS measures the cirrus areal extent and radiative properties. Special emphasis has been placed on developing and validating methods of detecting upper tropospheric clouds and defining their areal extent with infrared (e.g. 13.9 μm) and near infrared (e.g. 1.88 μm) channels; these are similar to the MODIS channels and MAS cirrus detection has direct relevance to the MODIS cloud mask algorithm.

Several studies have demonstrated the sensitivity of spectral radiances to cloud particle size and shape distributions. The MAS and HIS instruments provide accurate spectral measurements that can be used to assess differences in the radiative signatures between contrails and naturally occurring cirrus clouds. One difficulty in assessing the impact of high-altitude subsonic aircraft on cirrus formation and modification is the natural variability of the atmosphere and the potentially small signal of the radiative perturbation. Variations in the atmospheric spectral properties for contrail and natural cirrus conditions will be assessed with the two ER-2 instruments in conjunction with in situ and ground-based observations.

The Winter Cloud Experiment (WINCE January-February 1997) will investigate the difficulties in detecting cloud and estimating their properties in winter conditions. Cirrus and thin clouds over frozen tundra and lakes in the northern USA and Canada will be measured with the MAS and HIS (along with the GOES-8 and AVHRR). At least one of the missions will investigate the product stability in the transition from day (visible plus infrared) to night (infrared only) and then nighttime only. In addition two ground sites in New England will be instrumented for snow and ice cover measurements and MAS/HIS flights will be made in clear sky condition (in collaboration with Dorothy Hall and George Riggs working on the MODIS snow/ice product). The field campaign will be centered in Madison. Examples of the MAS cloud mask will be distributed to science team members so that they can determine its effect on their MODIS products.

FIRE, the First ISCCP (International Satellite Cloud Climatology Project) Regional Experiment, has previously conducted four successful field missions focused on cloud remote sensing and modeling studies as they relate to climate. FIRE Phase III will be conducted in the

Arctic in two phases, phase I to be conducted over a 7 week period or longer with a serial deployment of low- to mid-level aircraft, together with a 4 week period of high-altitude ER-2 overflights. During this component of FIRE III, it is anticipated that the University of Washington CV-580 and, to a lesser extent, the NCAR C-130Q will be utilized. Both of these aircraft will be equipped with an extensive set of PMS cloud microphysics probes, a Gerber PVM-100A liquid water content and effective radius probe, Johnson-Williams and King hot wire probes, a Nd:YAG lidar, thermodynamic state variable measurements, and selected chemistry instrumentation. In addition, the ER-2 will participate as the upper level aircraft from May 18-June 9, with the MAS, CLS, radiation measurement system for radiative fluxes, a multispectral along-track scanning radiometer, a microwave imaging radiometer. The primary sensors of interest to Goddard Space Flight Center (Michael King, Si-Chee Tsay, Steve Platnick, Robert Pincus) are the MAS on the ER-2, the CAR on the CV-580, and numerous in situ microphysics probes that will be invaluable in accessing the accuracy of cloud retrievals of the microphysical and radiative properties of Arctic stratus clouds over a bright (sea ice) surface. This valuable data set will also be of interest to the University of Wisconsin for testing the cloud mask algorithm, cloud phase and cloud top properties.

The first EOS-targeted campaign after the MODIS launch will be coordinated with measurements taken at the ARM site in Oklahoma, probably in September 1998. Another deployment the following spring is also planned. The ER-2 with MAS and HIS will be deployed to synchronize with the MODIS overflight; the ARM site suite of ground-based measurements (class-sonde, AERI, tower measurements of temperature and moisture at various elevations, microwave moisture measurements, lidar and radar observations, whole ski images) will be collected simultaneously. These combined air and ground measurements will be used to validate MODIS radiance measurements. Results will be used to adjust the infrared calibration coefficients as necessary. In addition, the ARM ground-based measurements can be used to validate geophysical parameters as well. Lidar and radar observations of cloud boundaries over the ARM sites will be used to validate the presence of a cloud as well as its cloud top pressure altitude. Whole sky imagers are also available at the site, and can be used to compare satellite and ground-based estimates of cloud amount. Finally, optical depth measurements derived from lidar

will aid in specifying the limit of thin cirrus detection in the cloud mask algorithm and for cloud properties.

An independent ground validation campaign of MODIS cloud heights will be undertaken six months after the MODIS launch (Fall 1998) through comparisons with stereo determinations of cloud heights (using the two GOES satellites over the U. S. and the University of Chicago ground all sky cameras), aircraft reports of cirrus cloud heights (from the ACARS), and lidar estimates of cirrus heights (using the University of Wisconsin lidar). These intercomparisons will be conducted in concert with a field campaign of the MAS on the ER-2 after the MODIS launch (probably at the time of the ARM overflights described above). Validation of the MODIS cloud emissivity will be attempted through comparison with the lidar determinations. Pre-launch validations will come from cloud top property determinations with MAS data from several field campaigns which will include stereo and lidar measurements as well.

The MOBY (Marine Optical Buoy) positioned near Lanai, Hawaii will be used in December 1998 to investigate MAS infrared-derived sea surface temperatures, visible/near-infrared water-leaving radiances, and radiometric calibration of the MAS measurements. The SST and water-leaving radiance data will aid in evaluating the results of several cloud mask spectral tests by providing accurate information on background radiance conditions. The effect of elevated water leaving radiances (caused by suspended materials or sub-aqueous bottom reflectance) on the cloud mask results will be investigated using MAS cloud mask results with MOBY water leaving radiances. MOBY data will also help assess temporal variability of water leaving radiance. MAS visible/near infrared calibration will be assessed by combining MOBY data with model-generated atmospheric scattered radiance. Well calibrated data are important for setting meaningful cloud mask test thresholds. Cloud investigation will be a by-product.

Once the MODIS is in orbit and returning regular data, we envision two focused periods of ER-2 overflights, to be coordinated with the EOS AM-1 orbit, in California (the first one over marine stratocumulus clouds located over the ocean between Monterey and San Diego in July 1999, and the second over valley fog in the central valley of California in December 1999). These

experiments would entail ER-2 flights from home base in California (either Ames Research Center or Dryden Flight Research Center), and would consist, once again, of the MAS and CLS, together with coordinated underflights by the University of Washington CV-580 with its in situ microphysics probes. This data set, of special interest to Goddard Space Flight Center (Michael King, Steve Platnick, Si-Chee Tsay) would help to validate the cloud optical thickness and effective radius between MODIS and the smaller spatial resolution airborne sensors on the ER-2.

3.2.3.a Validation of Cloud Top Properties Algorithm

The CO_2 slicing algorithm uses calibrated radiances that will be bias adjusted with respect to the NCEP forward calculations of clear sky radiances. Also the algorithm depends on the spectral radiance gradients or cloud forcing (clear minus cloudy fov radiances). These two considerations mitigate the algorithm dependence on extremely accurate calibration, although it is highly desirable.

As outlined in section 3.2.3 above, validation of the MODIS cloud heights will be undertaken through comparisons with stereo determinations of cloud heights (using the two GOES satellites over the U. S. and the University of Chicago ground all sky cameras), estimates of cloud height from cloud shadows, (using aircraft MAS, NOAA AVHRR, and GOES data), reports of cirrus cloud heights (from the ACARS), and lidar estimates of cirrus heights (using the University of Wisconsin lidar). These intercomparisons will be conducted in concert with field campaigns of the MAS on the ER-2 after MODIS launch. Validation of the MODIS cloud emissivity will be attempted through comparison with the lidar determinations. Pre-launch validations will come from cloud top property determinations with MAS data from several field campaigns which will include stereo and lidar measurements also.

Post-launch validation will be made by comparing the cloud top properties product with CERES single sample footprint (SSF) and single satellite gridded (SSG) products that include cloud top pressure and temperature. CERES is heavily dependent on MODIS observations for

cloud detection, so it will be important to ensure that the MODIS and CERES-derived cloud products are consistent. MISR altitude binned cloud fraction and stereo heights will be compared with the MODIS effective emissivity and cloud top heights to geometrically validate the MODIS radiometrically derived cloud height data.

3.2.3.b Validation for Cloud Phase Algorithm

The cloud phase algorithm uses calibrated radiances which will be converted into brightness temperatures, and averaged over a 5 x 5 pixel box. The use of temperature differences between the 8, 11, and 12 micron channels averaging also stresses the algorithm dependence on very accurate relative calibration between channels.

Validation of the infrared cloud thermodynamic phase product will be made primarily through comparisons with cloud lidar determinations (CLS onboard the ER-2) and cloud microphysical data (collected on instruments onboard the CV-580 and NCAR C-130Q) collected during field campaigns outlined in section 3.2.3 above. Limited pre- and post-launch validation will also be carried out using collocated HIRS/AVHRR data sets, focusing on surface emissivity effects. This data set has the advantage of its global coverage, but the spatial scale is far removed from that of MODIS, and the spectral bandwidths are wider and off center from those of MODIS. Post-launch validation will also consist of close inspection of sections of data representing differing cloud regimes and surface types, including cross checks during the day mode with the visible reflection function technique of King et al. (ATBD-MOD-05) and consistency with the cloud top properties results. Finally, post-launch validation will also include intercomparisons with other EOS instrument products such as the CERES SSF and SSG cloud phase product, and the ASTER polar cloud mask product, which includes a cloud phase bit.

3.2.4.a Quality Control of Cloud Top Properties Algorithm

As indicated in section 3.1.3.a., the accuracy of the cloud top pressures have been found to be 50 mb root mean square with respect to radiosonde, stereo, and lidar estimates; the effective emissivity determinations have been found to be correlate within 20% root mean square of lidar visible estimates of optical thickness.

Quality control within the software checks for cloud forcing greater than the instrument noise and cloud top pressure within the atmospheric layer where temperature and pressure enjoy a one to one relationship. Additionally, cloud top pressures will be stratified as a function of satellite viewing angle to make sure that the atmospheric transmittance corrections for viewing angle are not introducing a bias.

Beyond these simple tests, quality control is accomplished by manual and automated inspection of the data and comparison to other sources of cloud information. MODIS cloud top pressures and effective emissivities will be compared to those determined from the NOAA HIRS and the GOES sounder. Additional data from field experiments using the MODIS Airborne Simulator on the ER2 will assist with quality assessment of the MODIS cloud parameter determinations.

Global mean distributions of cloud height and emissivity will be compared from one week to the next; thresholds will be set to flag unrealistic changes. Trend analyses of global cloud properties will be compared with trends in OLR; a strong correlation between the two will be expected. Additionally comparisons with ISSCP will be made. These comparisons will all be done with the gridded .5 degree resolution MODIS cloud properties (determined from averaging of the 5 x 5 pixel cloud properties).

MODIS products will have an additional 8 bits of quality analysis information included for each product. Four of the bits will be the same for each product, the remaining 4 bits will be a quality indicator for the given product based upon expected results.

3.2.4.b Quality Control of Cloud Phase Algorithm

Quality control will consist of consistency checks with previous days resultant statistics, including the global cloud phase determination consistency and known cloud area persistence consistency (marine stratus regions, etc.).

MODIS products will have an additional 8 bits of quality analysis information included for each product. Four of the bits will be the same for each product, the remaining 4 bits will be a quality indicator for the given product based upon expected results.

3.2.5 Exception Handling

If the required radiance data is not available, then the algorithm will record the cloud products missing for that 5 x 5 pixel area.

3.2.6.a Data Dependencies of Cloud Top Properties Algorithm

The CO_2 slicing algorithm needs calibrated, navigated, coregistered one km FOV radiances from channels 29 (8.6 micron for moisture correction), 31 (11.03 micron infrared window), 32 (12.02 micron for moisture correction), 33-36 (13.335, 13.635, 13.935, and 14.235 microns CO_2 absorption band channels). Navigation implies knowledge of the surface terrain including height (DEM) and whether land or sea. The MODIS viewing angle for a given FOV must be known. The cloud mask from visible and infrared radiance considerations will be used as a indicator for cloud cover within a given one km FOV. The NCEP GDAS Final Run global model analysis of surface temperature and pressure as well as profiles of temperature and

moisture will be initially used in the calculation of the cloud forcing as a function of pressure and effective emissivity (in Equation (3)); as the AIRS/AMSU profiles become available, they will be used also. The Reynolds blended SST will also be used over the ocean. The algorithm also requires knowledge of the clear radiances for evaluation of the cloud forcing for each channel used in the ratio tests. This information will be provided in the form of clear radiance maps created and updated daily by the cloud mask production software. Table 3 summarizes the input data dependencies.

There has been some consideration for using the short wavelength CO_2 spectral bands 22 through 25 in parallel with the long wavelength CO_2 bands in a composite CO_2 slicing algorithm. The shortwave CO_2 algorithm has problems with reflected solar contributions during daylight hours, but is useful additional information at night. Current plans do not include these bands, but future versions of the software might.

Table 3. MODIS Cloud Parameter Input Data Dependencies

MODIS data channels	29, 31-36
Navigation	lat, lon, land, sea
MODIS viewing angle	lin, ele, ang
Cloud mask	yes, no, type
Surface data	SST, model analysis of temperature, dewpoint and pressure, topography (DEM)
Model profiles	temp (12 levels), moisture (6 levels)
Clear Radiance Base Maps	Channels 31, 33-36.

3.2.6.a Data Dependencies of Cloud Phase Algorithm

The tri-spectral cloud phase algorithm needs calibrated, navigated, coregistered one km FOV radiances (for FOV uniformity screening and conversion to brightness temperatures) from channels 29 (8.6 micron), 31 (11.03 micron) and 32 (12.02 micron). The MODIS viewing angle for a given FOV must be known. The MODIS cloud mask product will be used to screen areas

where the probability of cloud is high As the algorithm develops, a global surface emissivity map (related to surface cover) will be needed to adjust ice/water thresholds. Table 4 is a summary of the input data dependencies.

Table 4. MODIS Cloud Phase Input Data Dependencies

MODIS data channels	29, 31, 32
MODIS cloud mask	cloud or clear
Navigation	lat, lon, land, sea
MODIS viewing angle	lin, ele, ang
Surface data	surface emissivity

3.2.7.a Level 2 Output Product of Cloud Top Properties and Cloud Phase Algorithm

The Level 2 output file for each 5 x 5 pixel area (when cloud is present) is summarized in Table 5. The combined MODIS cloud properties, cloud phase and cloud retrieval product number is MOD06.

Table 5. MODIS cloud product (MOD06) Output File Contents

parameter number	content
1	day of observation
2	local time of observation
3	location latitude
4	location longitude
5	scan line number
6	scan element number
7	satellite zenith angle
8	solar zenith angle
9-28	brightness temperature of channels 27 through 36
29	flag for land or sea
30	flag for clear or cloudy
31-37	spectral cloud forcing for channels 29, 31 through 36
38	method of cloud height determination (CO_2 slicing or IR window)
39	cloud emissivity
40	cloud top pressure
41	cloud top temperature
42	cloud fraction
43	surface temperature
44	surface pressure
45-49	cloud height from the five ratios
50	cloud height from the IR window
51	tropopause height
52	flag for surface type
53-55	radiance variance for channels 29, 31 and 32
56-57	channel 29 minus channel 31 brightness temperature difference and channel 31 minus channel 32 brightness temperature difference
58	cloud phase code
59-62	Visible cloud retrieval product parameters (see ATBD-MOD-05) at 1 km resolution.

3.2.7.b Level 3 Output Product of Cloud Top Properties and Cloud Phase Algorithm

The Level 3 cloud top properties and cloud phase products will be included as part of a joint atmosphere discipline group product (MOD44). The products will be produced on a daily bases from the Level 2 files, on an 8 day basis from the daily files and a monthly bases from the daily Level 3 files. The Level 3 daily files will be produced at .5 degree equal area only, while the 8 day and monthly Level 3 product files are produced for both .5 degree equal area and .5 degree equal angle grids. The cloud top properties and cloud phase contribution to the joint product is shown in Table 6. An example of the probability of cirrus equal angle Level 3 product derived from HIRS data is provided in Figure 11.

Table 6. Cloud Top Property and Cloud Phase Level 3 Output File Contribution to Joint Atmosphere Level 3 Products

parameter number	content
1	thermodynamic phase (coded 0-6)
2	cloud top temperature
3	cloud top pressure
4	cloud top effective emissivity
5	probability of cirrus
6	probability of high cloud

3.3 References for sections 2 and 3.

Ackerman, S. A., W. L. Smith and H. E. Revercomb, 1990: The 27-28 October 1986 FIRE IFO cirrus case study: spectral properties of cirrus clouds in the 8-12 micron window. Mon. Wea. Rev., 118, 2377-2388.

Booth, A. L., 1973: Objective cloud type classification using visual and infrared satellite data. 3rd Conference on Probability and Statistics in the Atmospheric Sciences. Am. Meteor. Soc., Boulder, CO.

Chahine, M. T., 1974: Remote sounding of cloudy atmospheres. I. The single cloud layer. J. Atmos. Sci., 31, 233-243.

Eyre, J. R., and W. P. Menzel, 1989: Retrieval of cloud parameters from satellite sounder data: A simulation study. J. Appl. Meteor., 28, 267-275.

Gao, B.-C. and W. J. Wiscombe, 1994: Surface-induced brightness temperature variations and their effects on detecting thin cirrus clouds using IR emission channels in the 8-12 micron region. J. Appl. Met., 33, 568-570.

Gruber, A., and T. S. Chen, 1988: Diurnal variation of outgoing longwave radiation. J. Clim. Appl. Meteor., 8, 1-16.

Inoue, T., 1987: A cloud type classification with NOAA 7 split window measurements. J. Geophys. Res., 92, 3991-4000.

Inoue, T., 1989: Features of clouds over the Tropical Pacific during the Northern Hemispheric winter derived from split window measurements. J. Meter. Soc. Japan, 67, 621-637.

Jacobowitz, H. J., 1970: Emission scattering and absorption of radiation in cirrus clouds. Ph.D. thesis, Massachusetts Institute of Technology, 181 pp.

King, M. D., W. P. Menzel, P. S. Grant, J. S. Myers, G. T. Arnold, S. E. Platnick, L. E. Gumley, S. C. Tsay, C. C. Moeller, M. Fitzgerald, K. S. Brown and F. G. Osterwisch, 1996: Airborne scanning spectrometer for remote sensing of cloud, aerosol, water vapor and surface properties. J. Atmos. Oceanic Technol., 13, 777-794.

King, M. D., Y. J. Kaufman, W. P. Menzel and D. Tanre, 1992: Remote sensing of cloud, aerosol, and water vapor properties from the Moderate Resolution Imaging Spectrometer (MODIS). IEEE Trans. Geosci. Remote Sensing, 30, 2-27.

Menzel, W. P., W. L. Smith, and T. R. Stewart, 1983: Improved cloud motion wind vector and altitude assignment using VAS. J. Clim. Appl. Meteor., 22, 377-384.

Menzel, W. P., D. P. Wylie, and A. H.-L. Huang, 1986: Cloud top pressures and amounts using HIRS CO_2 channel radiances. Technical Proceedings of the Third International TOVS Study Conference, 13-19 August 1986, Madison, WI, 173-185.

Menzel, W. P. and K. I. Strabala, 1989: Preliminary report on the demonstration of the VAS CO_2 cloud parameters (cover, height, and amount) in support of the Automated Surface Observing System (ASOS). NOAA Tech Memo NESDIS 29.

Menzel, W. P., D. P. Wylie, and K. I. Strabala, 1989: Characteristics of global cloud cover derived from multispectral HIRS observations. Technical Proceedings of the Fifth International TOVS Study Conference, 24-28 July 1989, Toulouse, France, 276-290.

Menzel, W. P., D. P. Wylie, and K. I. Strabala, 1992: Seasonal and Diurnal Changes in Cirrus Clouds as seen in Four Years of Observations with the VAS. J. Appl. Meteor., 31, 370-385.

Parol, F. J., C. Buriez, G. Brogniez and Y. Fouquart, 1991: Information content of AVHRR Channels 4 and 5 with respect to the effective radius of cirrus cloud particles. J. Appl. Meteor., 30, 973-984.

Rossow, W. B., and A. A. Lacis, 1990: Global and seasonal cloud variations from satellite radiance measurements. Part II: Cloud properties and radiative effects. J. Clim., in press.

Smith, W. L., H. M. Woolf, P. G. Abel, C. M. Hayden, M. Chalfant, and N. Grody, 1974: Nimbus 5 sounder data processing system. Part I: Measurement characteristics and data reduction procedures. NOAA Tech. Memo. NESS 57, 99pp.

Smith, W. L., and C. M. R. Platt, 1978: Intercomparison of radiosonde, ground based laser, and satellite deduced cloud heights. J. Appl. Meteor., 17, 1796-1802.

Smith, W. L., H. M. Woolf, and H. E. Revercomb, 1991: Linear simultaneous solution of temperature and absorbing constituent profiles from radiance spectra. Appl. Optics, 30, 1117-1123.

Spinhirne, J.D., and W. D. Hart, 1990: Cirrus structure and radiative properties from airborne lidar and spectral radiometer observations. Mon. Wea. Rev., 2329.

Strabala, K. I., S. A. Ackerman and W. P. Menzel, 1994: Cloud properties inferred from 8-12 micron data. Accepted to the J. Appl. Meteor., March 1994 issue.

Susskind, J., D. Reuter, and M. T. Chahine, 1987: Cloud fields retrieved from analysis of HIRS/MSU sounding data. J. Geophys. Res., 92, 4035-4050.

Takano, Y., K. N. Liou and P. Minnis, 1992: The effects of small ice crystals on cirrus infrared radiative properties. J. Atmos. Sci., 49, 1487-1493.

Warren, S. G., 1984: Optical constants of ice from the ultraviolet to the microwave. Appl. Optics, 23, 1206-1225.

Wielicki, B. A., and J. A. Coakley, 1981: Cloud retrieval using infrared sounder data: Error analysis. J. Appl. Meteor., 20, 157-169.

Wu, M. L. and J. Susskind, 1990: Outgoing longwave radiation computed from HIRS2/MSU soundings. J. Geophys. Res., 95D, 7579-7602.

Wylie, D. P., and W. P. Menzel, 1989: Two years of cloud cover statistics using VAS. J. Clim., 2, 380-392.

Wylie, D. P. and W. P. Menzel, 1991: Two Years of Global Cirrus Cloud Statistics using HIRS. Technical Proceedings of the Sixth International TOVS Study Conference held 1-6 May 1991 in Airlie, VA, 344-353.

Wylie, D. P., W. P. Menzel, H. M. Woolf, and K. I. Strabala, 1994: Four Years of Global Cirrus Cloud Statistics Using HIRS. J. Clim., 7, 1972-1986.

4.0.a Assumptions of Cloud Top Properties Algorithm

The data is assumed to be calibrated (within the instrument noise), navigated (within one FOV), and coregistered (within two tenths of a FOV). The algorithm assumes the presence of only one cloud layer of infinitesimal thickness; adjustments for the presence of multiple cloud layers are under investigation. The cloud need not cover the entire FOV. Spectral cloud forcing must be greater than the instrument noise.

4.0.b Assumptions of Cloud Phase Algorithm

Assumptions are discussed in the estimate of error section 3.1.3.b.

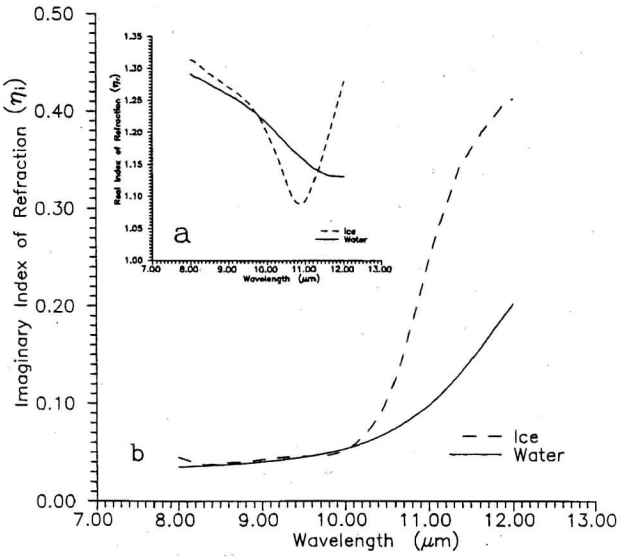

Figure 1. Indices of refraction of ice and water across the atmospheric window, (a) real portion, (b) imaginary portion.

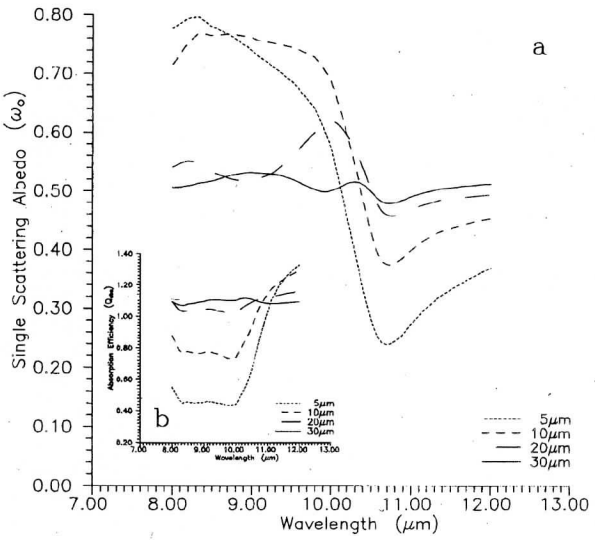

Figure 2. (a) Single scattering albedo of ice and (b) the absorption efficiency of ice, for four particle sizes (5,10, 20, and 30 microns), across the 8 to 12 micron spectral region.

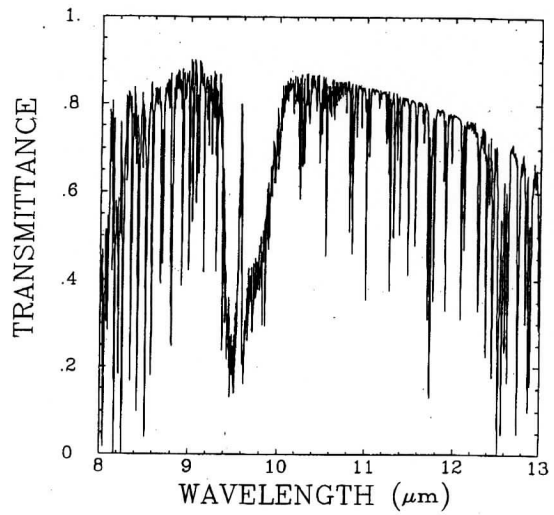

Figure 3. HIS total transmittance for a standard atmosphere across the 8 to 13 micron spectral region.

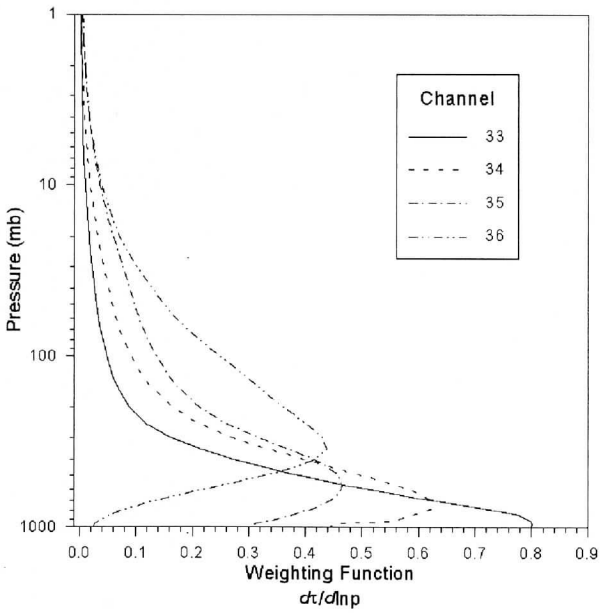

Figure 4. Weighting functions for the four MODIS channels in the CO_2 absorption band.

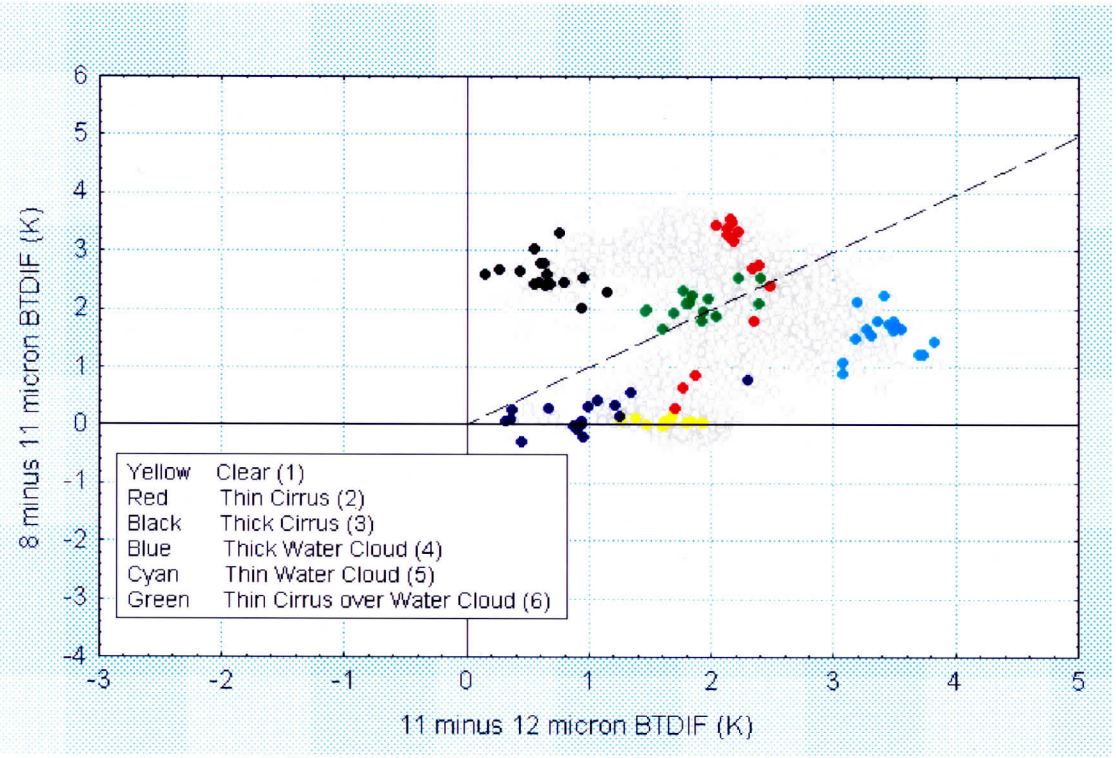

Figure 5. Scatter diagram of averaged brightness temperature differences 8 minus 11 micron versus 11 minus 12 micron of the multi-phase cloud scene of Figure 6 taken from the 5 December 1991 15:38 UTC MAS flight track data set. Points corresponding to the cloud types identified in boxes in Figure 6 are color coded.

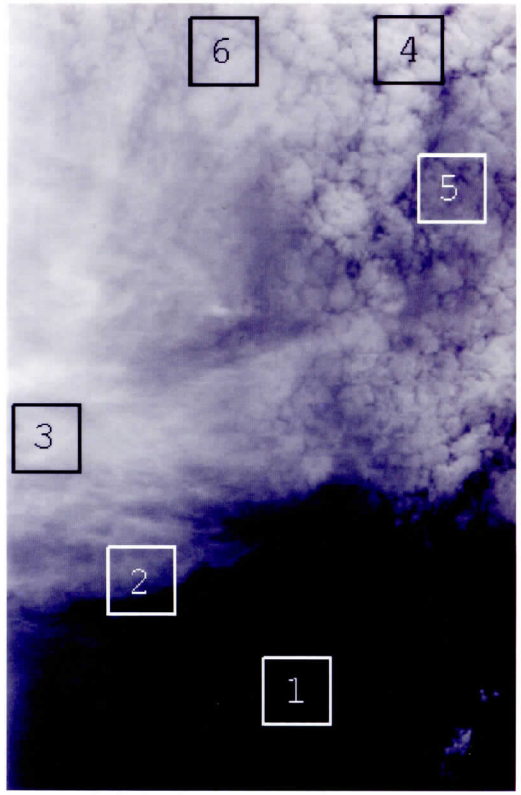

Figure 6. MAS mixed cloud scene 50 m resolution visible image from a portion of the 5 December 1991 data set at 15:38 UTC. Boxes represent differing cloud regimes color coded in the brightness temperature difference scatter diagram of Figure 5.

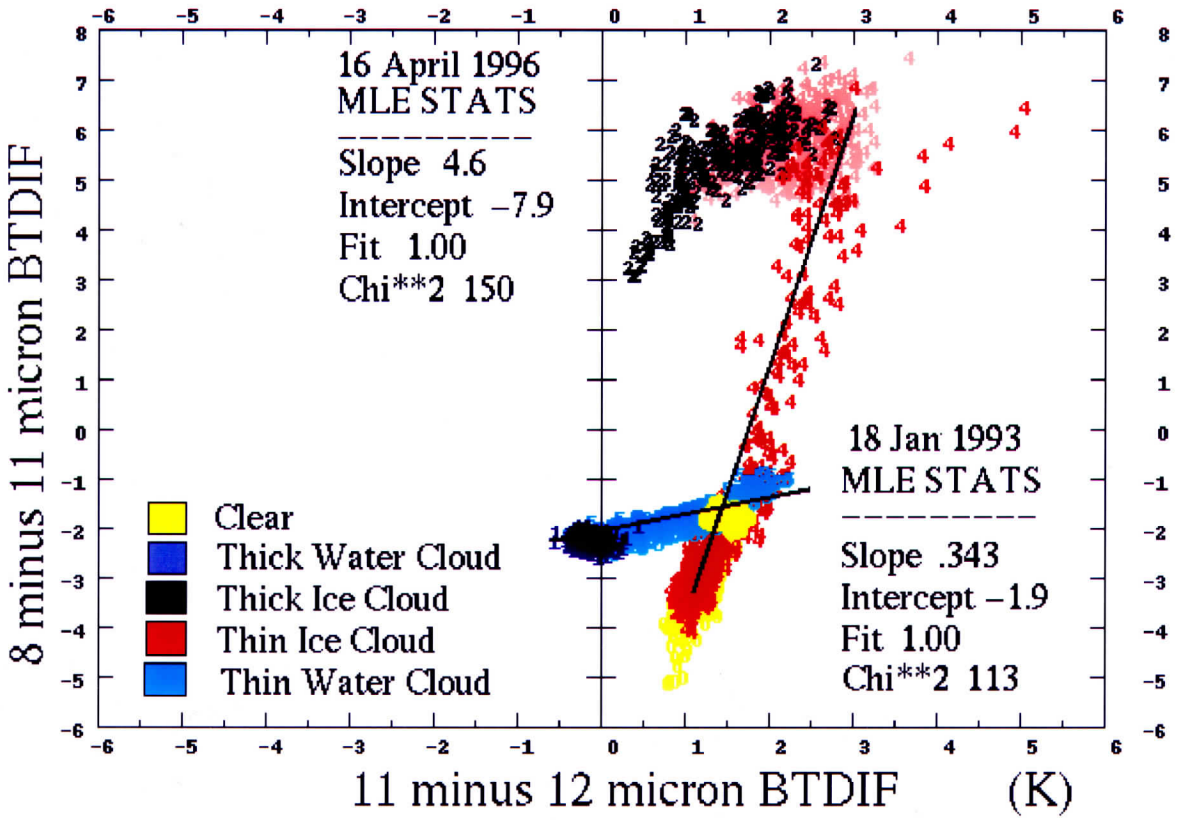

Figure 7. Scatter diagram of 8 minus 11 versus 11 minus 11 micron brightness temperature differences from an ice cloud (16 April 1996 SUCCESS) and water cloud (18 January 1993 TOGA/COARE) scene observed by the MAS instrument. Maximum Likelihood Estimator (MLE) statistics are included along with the final automated tri-spectral cloud phase determination for each 10 x 10 average pixel FOV. Only average FOV's whose brightness temperature was below 255 K are included in the MLE determinations. For the ice cloud case (red/pink/black), only the red points were used to determine the MLE statistics.

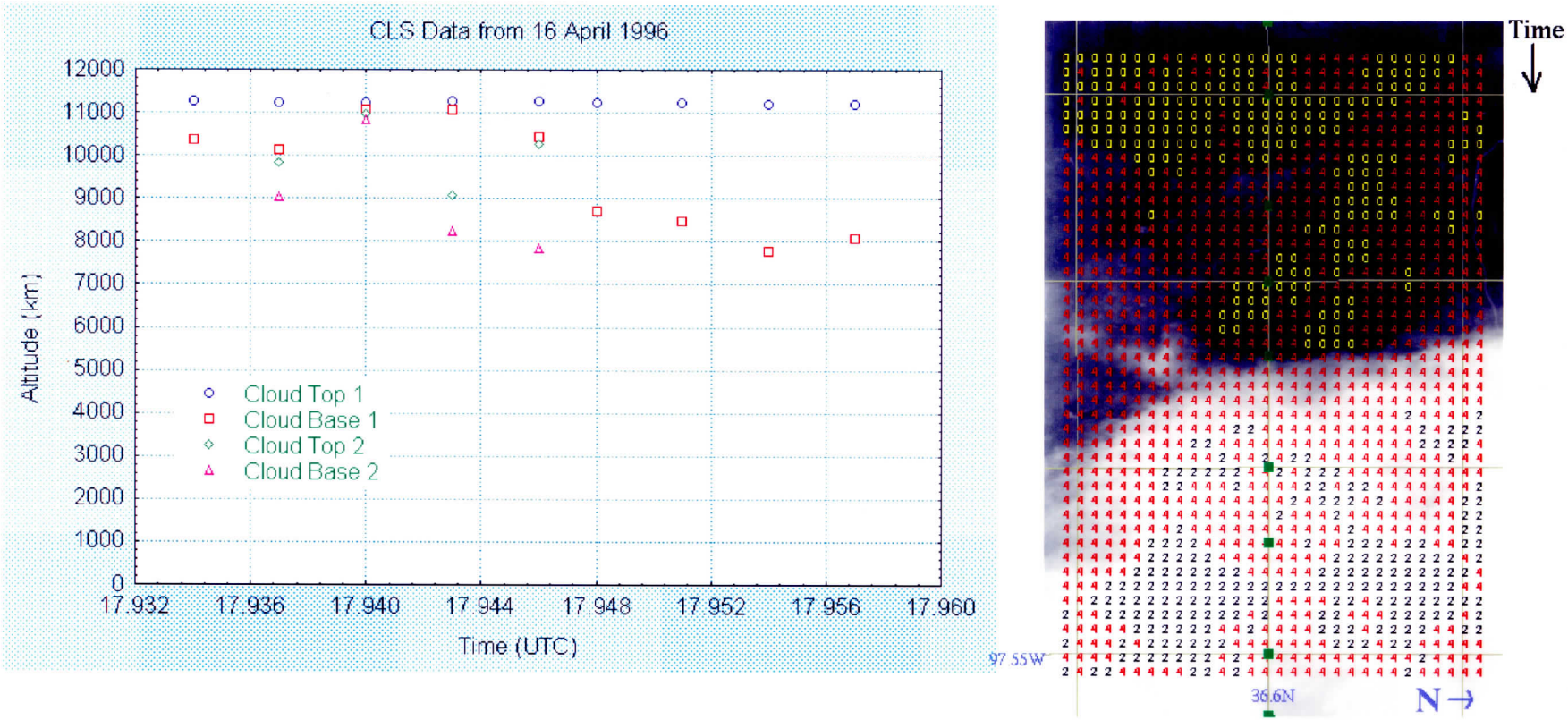

Figure 8. Cloud Lidar System (CLS) (Spinhirne 1990) cloud top and base estimates (left) and MAS 50 m resolution 11 micron image from the 16 April 1996 SUCCESS ER-2 flight. The MAS image is overlaid with the cloud phase coding determined from the tri-spectral technique shown in Figure 7. In this case, only ice cloud is detected (red/pink (4) and black (2)) along with some clear segments (yellow (0)). The collocated CLS observations are also indicted as green dots in the MAS image. Note how the CLS indicates high cloud with tops at around 11.5 km with variable bases. At times there are two cloud layers detected, but all bases are above 7.5 km. The cloud lidar image (not shown) also indicates cirrus cloud present.

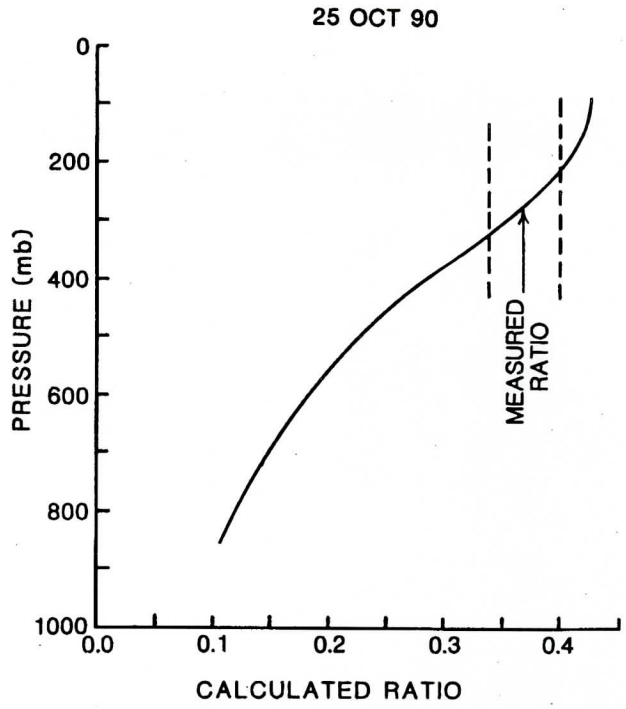

Figure 9. The calculated ratio from the right side of Equation 3 as a function of cloud top pressure from the sounding of 25 October 1990. The measured ratio from the left side of Equation 3 is indicated. The cloud top pressure is inferred to be 300 mb.

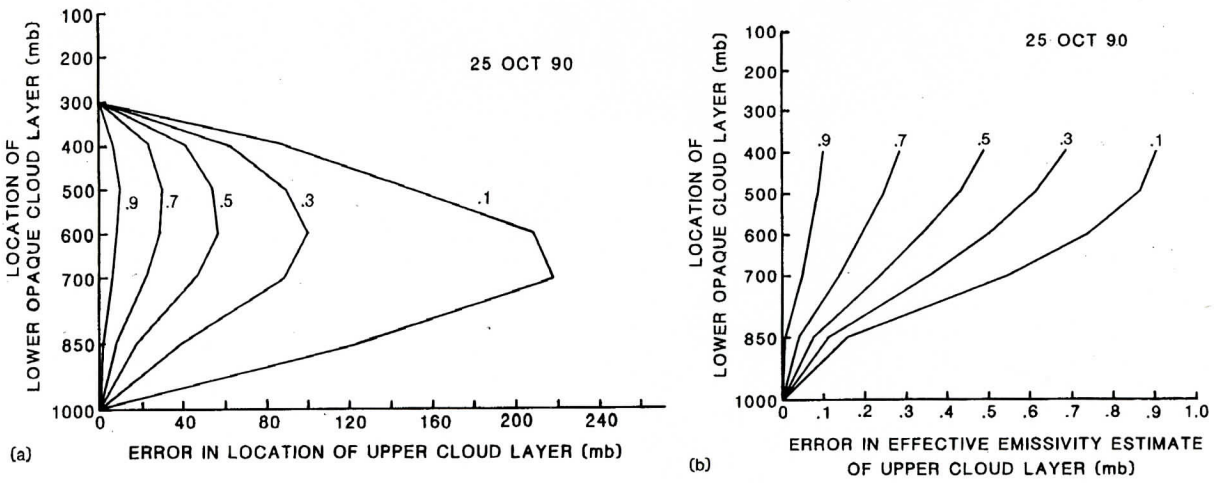

Figure 10. (a) The errors in calculated cloud top pressure (from the original 300 mb solution) for several different NE as a function of height of the underlying opaque cloud layer. (b) The associated errors in effective emissivity (from the original solution of NE).

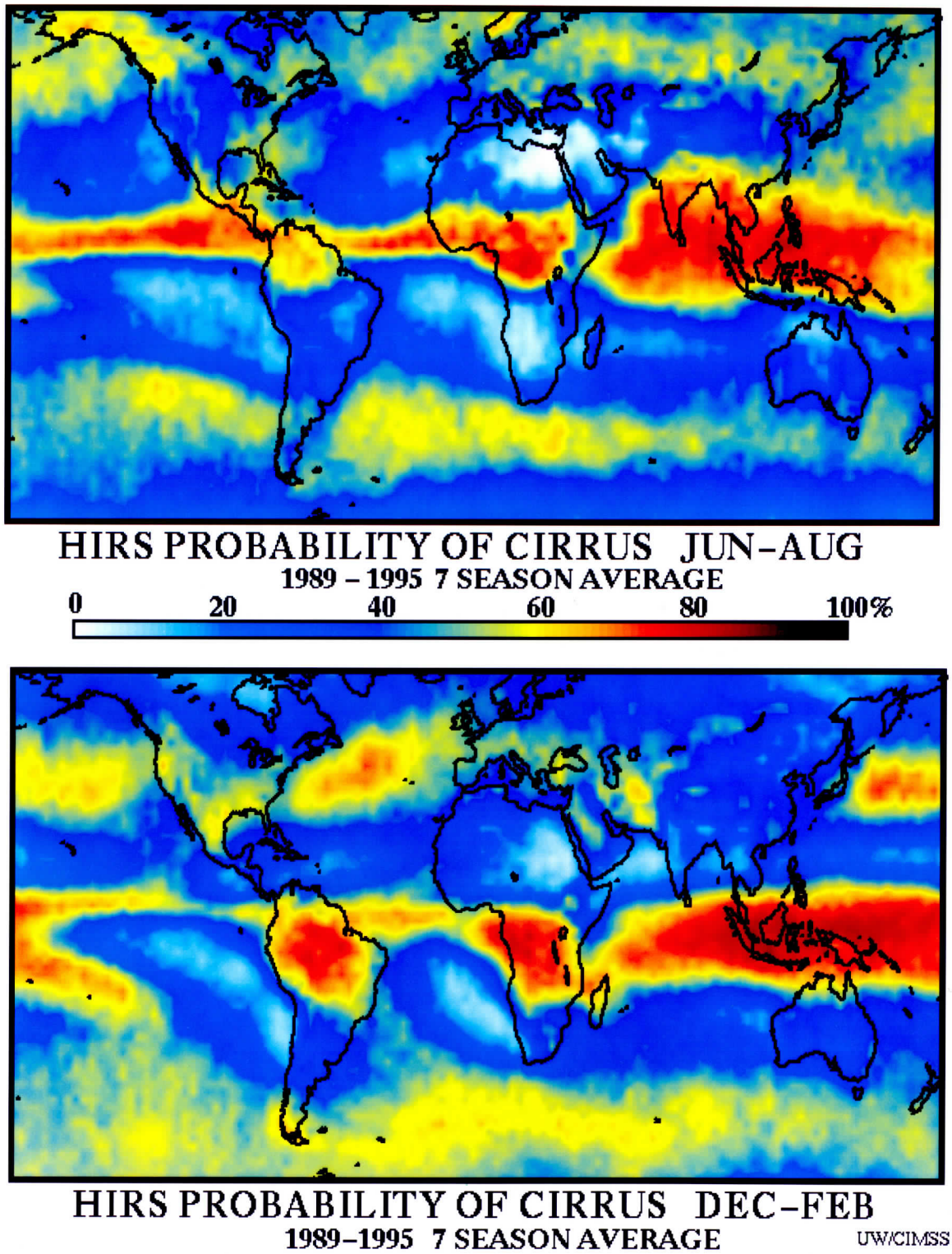

Figure 11. Example of a Level 3 equal angle cloud top property product as derived from HIRS data on a 2 degree latitude by 3 degree longitude grid.